Feasibility study of a non-contact, non-destructive testing method to assess the structural integrity of synthetic mooring ropes

Master's Thesis

J.W. Jongejan 4438191

TU Delft

Thesis for the degree of MSc in Marine Technology in the specialization of *Ship & Offshore Structures*

Feasibility study of a non-contact, non-destructive testing method to assess the structural integrity of synthetic mooring ropes

By

Jasper Jongejan

This thesis MT.23/24.018.M is classified as confidential in accordance with the general conditions for projects performed by the TUDelft.

14-02-2024

Thesis exam committee

Chair/Responsible Professor:	Dr. Pooria Pahlavan
Staff Member:	Dr. Apostolos Grammatikopoulos
Staff Member:	Filippo Riccioli Msc.
Staff Member:	Ir. Arno Huijer
Company Member:	Ir. Rigo Bosman

Author Details

Studynumber:	4438191

Cover image: delmarsystems.com, an artist impression of an offshore floating structure moored with a combination of steel chains and synthetic ropes.

Abstract

Governments are looking more and more to invest in renewable energy sources due to the energy transition that is currently taking place. One of the many renewable energy sources is wind energy which is increasingly positioned at sea. Wind turbines at deep parts of the ocean can be placed on floating structures which are often moored to the sea bottom by mooring ropes. For deep sea, the only viable option is a synthetic mooring line due to its almost neutral buoyancy.
Mooring ropes have a vital role in the offshore floating structure as it is keeping the structure in place. When a mooring line breaks, the consequences may be big, leading to serious damage or dangerous situations. Therefore, the structural integrity of mooring ropes should be evaluated regularly. For synthetic mooring ropes, the only method at this point in time is visual inspection. This can be done by divers or by Remotely Operated Vehicles (ROVs). This method is expensive, time consuming and in case it is done by divers, it is potentially dangerous. Furthermore, synthetic mooring ropes are susceptible to external damage which means inspection would have to be executed without direct contact with the mooring ropes. Therefore, it is necessary to assess the feasibility of a non-destructive, non-contact testing method in order to assess the structural integrity of a mooring line. The combination of non-destructive material property assessment and tension assessment is believed to produce a structural health monitoring instrument for synthetic mooring ropes.

In this thesis, a methodology is proposed which uses two independent non-contact, non-destructive measurements to assess the structural integrity of a high modulus polyethylene (HMPE) rope specimen. The measurements involved are ultrasonic guided wave (UGW) measurements and vibration measurements. The UGW measurements are performed to assess the stiffness of the test specimen according to the principle of attenuation of ultrasonic waves propagating through a specimen. The vibration measurements are performed to assess the natural frequencies of a manually excited test specimen. The assessed natural frequencies and the determined stiffness of the test specimen can be used to calculate the load acting on the test specimen.

The methodology is tested by conducting experiments in a laboratory environment where in-situ conditions are recreated by performing the tests underwater. For the experiments, a test specimen of DM20 HMPE rope is provided by Avient. The UGW measurements are performed by using ultrasonic transducers. One ultrasonic transducer transmits ultrasonic waves and two other transducers record the resulting ultrasonic wave over a set distance. Wave properties of the received wave are used to calculate the stiffness of the test specimen. The stiffness is compared to the reference stiffness provided for DM20 and is in good agreement. The vibration measurements are performed using a Laser Doppler Vibrometer (LDV). An LDV is capable of contactless measuring vibrations of a vibrating object by using the Doppler principle. The test

specimen is manually excited by an impact hammer while the specimen is under tension. The LDV measures the response of the test specimen. From this response, the natural frequencies of the test specimen at different loads can be determined. The measurements are used according to the methodology to recalculate the loads the test specimens are subjected to. It was concluded that the loads can be recalculated with varying accuracy of approximately 10% with respect to the theoretical values, with increasing accuracy for higher load values. It was concluded that the proposed methodology has the potential to determine load on a synthetic mooring line, but there are uncertainties in the results due to inaccuracies in the experiments. Due to these inaccuracies, some of the variables have been estimated by implementing the literature value. For future research, it is suggested to improve the quality of the experiments in order to make the results more reliable.

Contents

List of Figures

Nomenclature

Acronyms

HMPE	High Modulus Polyethylene
LDV	Laser Doppler Vibrometer
MBL	Minimum Breaking Load
ROV	Remotely Operated Vehicle
SHM	Structural Health Monitoring
UGW	Ultrasonic Guided Wave

Greek Symbols

α	Attenuation coefficient	m^{-1}
ϵ	Strain	–
ω	Temporal frequency	Hz
ρ	Density	$\frac{\mathrm{kg}}{\mathrm{m}^3}$
σ	Stress	Pa

Roman Symbols

A	Area	m^2
a	Amplitude of signal	V
a_0	Amplitude of reference signal	V
c	Wave speed	$\frac{\mathrm{m}}{\mathrm{s}}$
C_a	Added mass coefficient	–
d	Distance	m
E	Stiffness	GPA
F	Force	N
f_n	Natural frequency	Hz
g	Gravitational constant	$\frac{\mathrm{m}}{\mathrm{s}^2}$

I	Area moment of Inertia	m^4
k	Wave number	m^{-1}
k^*	Complex wave number	m^{-1}
Kr	Non-dimensional stiffness parameter	–
L	Length	m
m	Mass	kg
m_a	Added mass per unit length	$\frac{\mathrm{kg}}{\mathrm{m}}$
m_s	Structural mass per unit length	$\frac{\mathrm{kg}}{\mathrm{m}}$
n	Number of vibration mode	–
S	Force	N
T	Tension	N
t	Time	s
u	Amplitude	m
u_0	Half peak-to-peak amplitude	m
V	Volume	m^3
v	Speed	$\frac{\mathrm{m}}{\mathrm{s}}$
w	Weight per unit length	$\frac{\mathrm{N}}{\mathrm{m}}$
x	Horizontal position	m
y	Vertical position	m

1 Introduction

1.1. Background and motivation

In December 2015, close to 190 countries adopted the Paris Agreement [1]. In order to achieve the goals of the Paris agreement, a shift from fossil energy towards renewable energy has been taking place which is known as the energy transition. It is expected that electricity will have a 50% share of the total energy mix in 2050 of which 83% will be generated by renewable energy sources. With this, it is expected that the share of wind energy will grow from 1% in 2020 to 13% in 2050 of the total renewable energy produced [2]. In order to facilitate this high interest in wind energy, governments have been investing in offshore wind farms in the recent years [3]. Offshore wind farms can be found in different parts of the ocean. In shallow water, they can be connected to the bottom using bottom fixed structures. Bottom fixed wind farms are usually viable with depths up until 50-60 meters. In deeper water, up until 700 meters, floating offshore structures are the preferred alternative [4]. Floating offshore structures such as floating wind turbines and floating solar parks are typically moored to the seabed using mooring ropes. The most common types of mooring ropes are steel chains, steel wire and synthetic ropes.

Synthetic mooring ropes

The main advantage of synthetic ropes over steel wire and steel chains is their material density [5]. Synthetic ropes have almost neutral buoyancy having a density of approximately 970 $\frac{kg}{m^3}$ compared to a density of 7850 $\frac{kg}{m^3}$ for steel. The high density of steel wire and steel chains makes them significantly heavy and costly when used in deep sea applications [6]. Another advantage of synthetic ropes over steel wire and chains is the fact that synthetic ropes can absorb energy in cyclic loading which leads to the ability to absorb energy during snap load events [7]. The physical reason for this is the fact that synthetic materials show time-dependent viscoelastic and viscoplastic behaviour which is dependent on load history, load rate, load amplitude and mean load [8]. Finally, synthetic ropes experience no corrosion, have better tension fatigue performance, out-of-plane loading and torsion performance than steel components [9].

Synthetic mooring ropes are relatively sensitive to damage. Synthetic ropes are made of individual strands and yarns which may be damaged due to sliding over rough or

sharp surfaces or they might get caught behind sharp objects such as nails or burs [5]. A defect beginning in one of the yarns may grow over time and result in the failure of the rope as a whole if the defect goes unnoticed [5]. Therefore, it is important to avoid unnecessary contact with the rope while in service or during handling.

Incidents with synthetic mooring ropes

The integrity of mooring ropes is important for offshore floating assets as these structures prevent floaters from drifting away. Mooring line failure can be prevented by in-situ inspection. However, even though mooring ropes are often visually inspected during their life time, several incidents have happened over the years [10], [11]. This also includes incidents with synthetic mooring ropes [10], [12]. In case of severe incidents, the consequences may be catastrophic leading to high damage and dangerous situations.

In May 2002, 3 of 9 mooring ropes of the Girassol buoy failed [10]. The mooring ropes were made from a combination of steel chains and polyester rope. One of the three ropes failed in the polyester rope part which caused the buoy to drift slightly leading to the other line failures. It was later determined that the failed polyester rope had a pre-existing cut which was not detected during inspection using a remotely operated vehicle (ROV). The buoy drifted out of the design envelope without damage to the oil offloading lines.

A second example is an incident which occurred on 13 September 2012. The Transocean Barents experienced a fibre rope failure at 350 meter from the unit during testing [11]. It was believed that the reason the rope failed was due to the rope moving along a fixed (sharp) object even though no obvious cause could be found.

A third example of an incident including a broken synthetic mooring rope occurred on 25 November 2011. Operators of the Transocean Winner semi noticed a significant drop in the load in one of the synthetic anchor ropes. This indicated a broken mooring rope [11]. As a result, the rig moved 15-20 meters from the original position. The location where the mooring rope failed experienced high friction and possibly bending during handling which may have contributed to the failure of the mooring rope.

1.2. Collaboration partner

Avient is a company specialised in polymer materials. In this thesis, they will assist in providing High Modulus Polyethylene (HMPE) rope material for tests alongside their extensive knowledge on HMPE materials. There are multiple examples of materials designed and produced by Avient in the field. One example is the mooring ropes on the Stiesdal TetraSpar near the coast of Norway [13]. This is a commissioned and fully operational project operating in 200 meters deep water. The TetraSpar uses winch lines made with Dyneema®SK99 and is moored with Dyneema®DM20. The conclusions drawn from this project were that DM20 synthetic mooring ropes show negligible creep deformation.

Another example is the WindFloat Atlantic project off the coast of Portugal [14]. This project is the first project in which Dyneema®DM20 HMPE ropes are used for permanent mooring. In this project, the synthetic rope was incorporated as a middle rope

meaning that the synthetic rope was situated between the catenary bottom chain and the platform itself. The conclusions of the project were that the DM20 mooring ropes offer a lightweight solution for mooring while offering lower pre-tension with the same station keeping performances. Furthermore, it was shown that the fatigue life time of the DM20 synthetic rope shows good performance.

1.3. Objective

In order to improve the reliability and safety of mooring systems, a quantitative and detailed inspection technique is required. Currently, the only adequate and allowed inspection method for this is visual inspection (according to DNV Rules and Standards DNV-RP-E304 [15]). This is a time consuming, expensive and possibly dangerous method. Furthermore, the mooring rope failure of the Girassol buoy showed that visual inspection using a ROV is not reliable enough to prevent failure sometimes. Therefore, it is necessary to find alternative ways of structural integrity assessment of synthetic mooring ropes. Due to the vulnerable nature of synthetic ropes, it is important to avoid direct contact with the material in order to prevent initial damage. Load in mooring ropes is often monitored in order to assess the structural integrity of a mooring rope. However, this is often done using the intrusive load cell method [16] whereas a non-contact solution is more suitable for synthetic mooring ropes. The goal of this research is therefore defined as follows:

The goal of this research is to formulate a methodology to assess stiffness and tension of loaded synthetic ropes using non-contact assessment techniques which can be applied in-situ.

1.4. Research Question

The goal of this research leads to the following research question:

”How can material properties and tension of synthetic mooring ropes be assessed using a non-contact combination of ultrasonic guided waves and vibration measurement?”

In order to answer this research question, a methodology should be formulated. The methodology shall be divided into wave propagation measurement and vibration measurement in order to assess the stiffness and tension in the synthetic mooring rope. This leads to the following subquestions.

”What kind of test methodology can be used in order to measure wave propagation in a synthetic mooring rope in a non-contact manner?”

”How can non-contact vibration measurements assess tension in synthetic mooring ropes?”

It is known that synthetic materials show viscoelastic and viscoplastic behaviour. It is also known that these properties may have an influence on the wave propagation characteristics. Furthermore, it is also known that loading may have an effect on wave propagation. Therefore, the following two additional subquestions shall be answered.

”How does viscoelasticity affect ultrasonic wave propagation in synthetic mooring ropes?”

”How does tension affect ultrasonic wave propagation in synthetic mooring ropes?”

1.5. Lay out of the report

This report is divided into 7 chapters. In chapter 2, the relevant literature is briefly discussed. In chapter 3, the methodology is proposed. The experimental setup will be shown in detail in chapter 4. The results following from the experiments will be shown in chapter 5. In chapter 6, the conclusions of the research will be presented by answering the research question. Recommendations for future research will be given in chapter 7.

2

Literature Review

2.1. Structural integrity assessment of synthetic mooring ropes

Damage generally leads to changes in mechanical and electromechanical properties of structures. Structural Health Monitoring (SHM) techniques translate these changes into integrity status of the structure. SHM can enable the detection of the onset of new damage and/or the progression of an active area. This can prevent failure [17].

Prevention of failure is economically beneficial and ensures safety. SHM techniques used for (synthetic) mooring lines can be divided into failure assessment techniques and structural integrity assessment techniques. The failure assessment techniques can be summed up as [18]:

- Sonar probe system
- Inclinometer
- Global positioning system and gyro
- Indirect in-line tension monitoring
- Integrated monitoring and advisery system

In general, these techniques measure either the position of the floating structure or the angle of the mooring lines with respect to the floating structure in order to assess whether a mooring line has failed [18]. As failure assessment implies, the mentioned techniques can only be used to assess whether one or more mooring lines have failed. Since the goal of this research is to establish a technique to assess the structural integrity of synthetic mooring ropes before they fail, the mentioned failure assessment techniques will not be considered.

Currently, the only structural integrity assessment method that is allowed to be used is visual inspection (according to DNV Rules and Standards DNV-RP-E304 [15]). Visual inspection is either performed by divers or by ROV. During inspection, the synthetic mooring line is checked for initial faults and visible damage. This method is deemed

expensive, time consuming and potentially dangerous in case divers perform the inspection [18],[19].
Besides visual inspection, there are four main promising alternatives for structural integrity assessment of synthetic mooring ropes. These are load cell measurements [20], acoustic emission [21], ultrasonic guided waves [22] and vibration analysis [23]. Note that load cell measurements and vibration analysis are focused on tension assessment while acoustic emission analysis and ultrasonic guided wave analysis are focused on damage identification and material properties assessment.

2.1.1. Damage mechanisms of HMPE mooring ropes

The main damage mechanisms of synthetic mooring ropes are abrasion, bending and creep. Additionally, UV exposure and marine growth can contribute to degradation of material.

Abrasion

Abrasion is described as yarn on yarn abrasion meaning that wear on individual yarns is introduced due to abrading over one another. Sheng et al. (2021) [24] performed an experiment to study the thermal and mechanical wear phenomena during the yarn on yarn abrasion. They concluded that the wear of fibers is the most prominent phenomenon that weakens the fiber during yarn friction. They found that the yarn surface generates hairiness when abrading, eventually leading to fiber failure. Furthermore, it was concluded that the abrasion leads to local heating of the yarns. This can cause fiber bundel nodulation causing a decreased abrasion resistance. Finally, it was concluded that initial production flaws in the fiber are usually the starting point of cracks. Vlasblom et al. (2012) [25] concluded that DM20 performs very well when it comes to yarn on yarn abrasion. It was concluded that DM20 passes the minimum requirement for yarn on yarn abrasion set by the American Bureau of Shipping. Furthermore, it is known that the external abrasion can be well avoided by using a HMPE external abrasion protection cover [14]. Polyester and DM20 have comparable abrasion performances [14], [9]. Nylon typically performs worse compared to polyester [26]. However, a recent study from Chevillotte et al. (2020) [27] showed that the abrasion resistance of nylon ropes can be significantly improved by adding a coating to the rope. By adding the coating, they found a better fatigue performance than steel chains but it still showed that the fatigue performance due to abrasion of nylon ropes was worse than for polyester ropes.

Bending

Bending fatigue occurs because synthetic mooring ropes are run over sheaves and winded on drums at the connection to the offshore floating platform. Running over sheaves and winding on drums leads to bending stresses beside the tensile stress in the rope [28]. During testing, the bending fatigue life time is measured by looking at the performance when it is guided over sheaves. This is mainly important for vertical mooring configurations. There are a number of studies in which the bending stiffness of HMPE is evaluated. Wehr, Pott and Wehking (2018) [28] evaluated the bending performance of HMPE ropes compared to steel wire. For this, they plotted the life time of the specimens to the diameter related force S/d^2 in which S is the force and d is the diameter of the specimen. They found that HMPE ropes have good bending

performances. For relatively low diameter related force values, the ropes only had a slightly smaller life time while for relatively high diameter related force values, the ropes performed as good as the steel wire.

Finally, the performance of DM20 compared to steel wire and other HMPE ropes was evaluated by Davies et al. (2018) [29]. The performance of DM20 was compared to Dyneema SK78. This is another type of HMPE rope which was the precessor of DM20 and has a lower creep resistance than DM20. In the research, the HMPE ropes were coated with two coatings: XBO and DPX. These coatings are used to improve the bending life time of the ropes. It was found that DM20 coated with XBO has better bending fatigue performance than SK78 coated with XBO. Furthermore, it was shown that DM20 coated with XBO has a five times better bending fatigue performance than steel wire with the same diameter.
Finally, the bending performance of nylon and polyester is worse than Dyneema HMPE ropes [5].

Fatigue behaviour of nylon and polyester
Failure mechanics due to fatigue are comparable for nylon and polyester. In both materials, cracks initiate at the surface or just below it. After that, cracks will propagate in axial direction of the fiber producing long fatigue cracks [30].

Fatigue behaviour of nylon and polyester has been researched extensively in the 1980's and more recent already [31], [32], [33]. All researches compared the fatigue behaviour of nylon and polyester. They concluded that nylon and polyester have comparable fatigue performances when single fibers are used. This is however complicated to compare due to the much lower stiffness of polyester [33]. The study of Chevillotte et al. (2020) [33] for example used a load control which led to the conclusion that the fatigue performances of nylon and polyester were comparable. It was noted that the results may be different if a strain control was used for the comparison. However, the studies of Kenney, Mandell and McGarry (1985)[31], Mandell (1987)[32] and Chevillotte et al. (2020)[33] also showed that the fatigue data rather changes when full ropes rather than single fibers are used. It was found that polyester performed much better than nylon when looking at fatigue performance of full size ropes.
It should be noted that in general, fatigue life time of nylon is shorter than that of polyester for the same applied load as was found by Seo et al. (1997) [34]. Figure 2.1 shows this phenomenon. The reason for this is the fact that abrasion resistance of nylon is lower than the abrasion resistance of polyester. During cyclic loading, fibers will abrade over one another initiating fiber cracks.

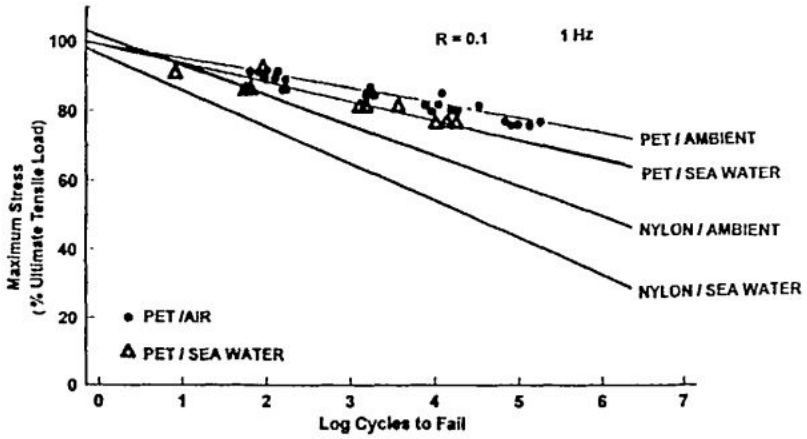

Figure 2.1: Nylon and polyester fatigue behaviour for wet and dry yarns [34].

Fatigue behaviour of HMPE

Fatigue behaviour of HMPE ropes is governed by the creep behaviour of them [35], [36]. The creep behaviour of HMPE ropes is different from polyester ropes. Figure 2.2 shows a typical creep curve for both HMPE and polyester.

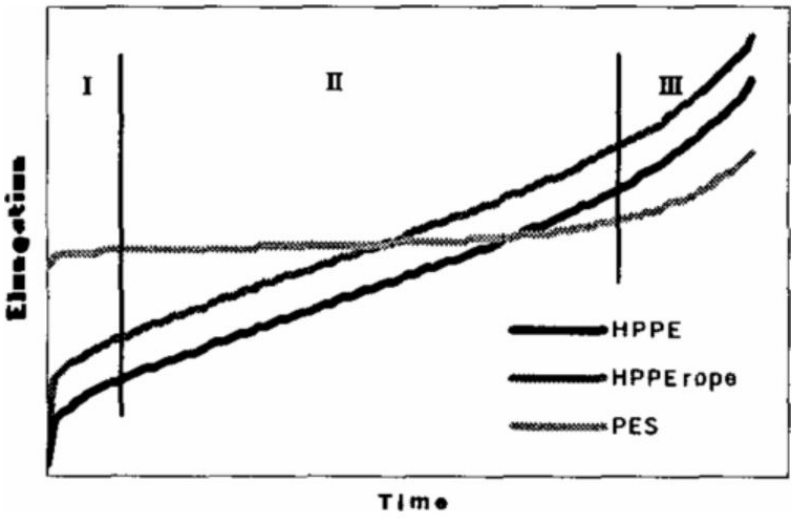

Figure 2.2: Creep curves (elongation vs time) of HMPE compared to polyester. Note that polyester is refered to as PES and HMPE is refered to as HPPE [36].

Three creep regimes can be observed.

- Stage 1 is the reversible elastic and delayed elastic elongation. HMPE has a low elongation upon failure (generally 1.5-3%) while polyester has a much higher elongation upon failure (generally 10-25%).Both materials show a primary creep deformation characterised by a decreasing creep rate. Primary creep is fully reversible upon unloading [36].
- Stage 2 is the secondary creep in which the creep rate is approximately constant. Differences between polyester and HMPE arise in stage 2 because this stage

is irreversible for HMPE while for polyester it is not clear whether it should be regarded as very small irreversible creep or as delayed elastic elongation [36].

- Stage 3 is tertiary creep and is fully irreversible for both polyester and HMPE. The creep rate increases again and polymer chains start to break leading to failure of the rope [36].

Since creep is a known problem for HMPE ropes, research has been performed in order to produce new HMPE material for ropes which show significantly less creep [25], [37]. This type of HMPE fiber is known as DM20 which is the material which is provided by Avient for this research. This material shows better creep performance compared to conventional HMPE fibers. Since creep is the governing fatigue failure mode for HMPE ropes, DM20 has a highly increased life time compared to other types of HMPE. This makes HMPE ropes more suitable for offshore mooring applications even though it has limitations. The high stiffness properties make them less suitable in a storm. During a storm, the mooring ropes need stretch in order to maintain storm survivability. To overcome this potential issue, often times these mooring systems are made out of a combination of different materials leading to hybrid ropes. A hybrid rope may be build up out of HMPE ropes in order to provide stiffness and better fatigue performance, while parts of the rope are made from polyester in order to provide the necessary stretch in case of storm loading [25].

UV exposure

Weller et al. (2013) [38] states that UV exposure to the outer fibers of a synthetic rope will lead to material degradation over time. This leads to brittle and discoloured fibers at the outer surface which will be weaker than the undamaged inner fibers of the rope. For synthetic ropes submerged in sea water, the UV exposure decreases with depth. The UV resistance of HMPE fibers is limitedly researched. Bosman et al. (2020) [14] touched upon the principle of UV degradation by saying it has an influence on HMPE ropes without quantifying the effect. The handbook of Vlasblom (2018) [39] gives some guidance on degradation of HMPE fibers due to UV. From this, it is known that the HMPE needs no specific precautions when exposed to UV for shorter periods of time. However, it does have a influence on the material. Especially for longer periods of time, the influence is measurable. Long exposure results in a decrease in tenacity (the breaking load divided by mass per unit length) and elongation at break. However, the modulus of the fibers is almost unaffected. Finally, it is indicated that the colour of HMPE fibers has an influence on the UV resistance. Black types of HMPE fibers have a two to four times better UV resistance compared to white types. Finally, the ropes can be protected to UV by means of a cover due to the fact that UV-light only penetrates the material by one to four millimeters. The influence of seawater on UV penetration in the material is not evaluated[39], [5].

Marine Growth

Marine growth can influence the rope performance by influencing its strength and by adding weight to the rope itself. In the study of Bosman et al. (2020) [14], it was found that Dyneema fibers have the lowest amount of marine growth on it compared to other

fibers. The fibers do not degrade as it is no food for marine life. Near the surface of the water, mussels can start to grow on the ropes but research indicated that this has no substantial effect on the strength of the rope. Therefore, marine growth is no major degradation method for HMPE ropes.

2.2. State of the art

Load cell

There are several examples in which the load cells have been used in order to assess the load on mooring ropes [40], [41], [16]. Often, strain gauge based load cells are used which measure the small strain acting on the load cell due to the load exerted on it. Load cells have been used for research of load measurement of mooring lines in the past. Huang, Tang and Wang (2010) [40] measured the load on mooring lines of a floating structure during a typhoon using a load cell. With the load cell, they determined the mean and peak loads on the mooring lines in an accurate manner. The advantages of load cells are that it is a relatively well established technology and that the resulting load output is a direct measure of the structural health of the mooring line. However, load cells do have a number of disadvantages. The main disadvantage is that the load cell shall always be positioned between the mooring line and the fairleads of the floating structure. This means that load cell measurement is an intrusive measurement technique which does not comply with the research objective.

Acoustic emission

Acoustic emission of steel wire mooring lines have been researched in the past [21], [42], [43]. Casey, White and Taylor (1985) [43] researched acoustic emission in steel wire ropes and concluded that the acoustic emissions recorded by the transducers can be related to the number of wire breaks within the rope. The research was performed in a laboratory setting. A follow up of this research was performed by Casey, Holford and Taylor [42]. In this research, the steel wire ropes were submerged in water in a laboratory environment. It was concluded that acoustic emissions can both be detected by direct contact between the receivers and the rope, or in a non-contact situation. It was however concluded that the signal duration is reduced in a non-contact situation compared to the direct contact situation. Drummond et al. [21] performed similar research in 2007. In this research, undamaged specimens and damaged specimens were used. During the initial phase (in which no damage was applied), the number of counts and hits was significantly higher than during the final phase (in which the damage was applied). The hits in the final phase were of high amplitude. Additionally, they had a large number of counts and greater energy compared to the hits in the initial phase. Therefore, they concluded that hits of high amplitude with great energy indicate failure of a wire.

Ultrasonic guided waves

Studies into non-destructive testing of rods submerged in water using ultrasonic guided waves were performed in the 1990's [22], [44], [45], [46]. Dayal (1993) [46] described the change of dispersion relations for rods submerged in water. Furthermore, this research described the change of attenuation between the two cases. There is a change in attenuation due to energy of the ultrasonic wave leaking to the water sur-

rounding the rod. It was concluded that submerged bars with a relatively high density have lower attenuation compared to submerged bars with a relatively low density. Furthermore, it was concluded that the stiffness of a material has an influence on the attenuation. A higher stiffness leads to a lower attenuation. Figure 2.3 shows the attenuation curves for both a magnesium rod submerged in water and a glass/epoxy rod submerged in water. The density of magnesium is slightly lower than glass/epoxy which should lead to a higher attenuation for magnesium. However, due to the fact that the magnesium rod has a higher stiffness, the attenuation of the magnesium rod is in fact slightly smaller than the attenuation of the glass/epoxy rod. This can be seen in figure 2.3.

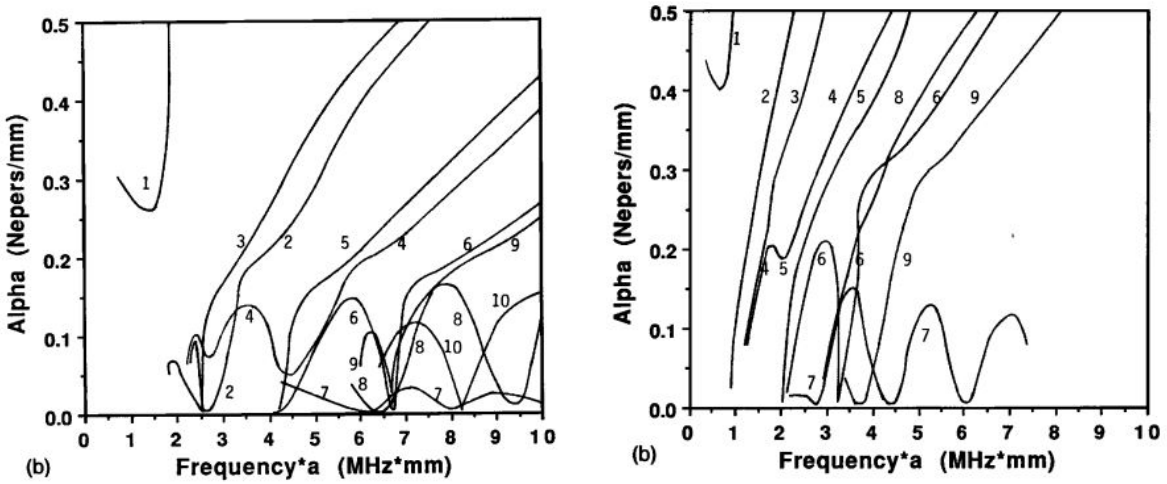

(a) Attenuation curves for magnesium rod submerged in water. (b) Attenuation curves for glass/epoxy rod submerged in water.

Figure 2.3: Attenuation curves of magnesium rod and glass/epoxy rod submerged in water [46].

Important to note in this context is the fact that synthetic fiber ropes have a changing stiffness under changing load. Davies et al. (2002) [47] defined a non-dimensional stiffness parameter Kr which is calculated as follows:

$$Kr = \frac{\Delta F/MBL}{\Delta \epsilon} \tag{2.1}$$

The research showed that the stiffness parameter Kr would increase with increasing load as may be seen in figure 2.4. This is an important conclusion as Dayal [46] showed that increasing stiffness leads to a lower attenuation of the ultrasonic guided waves.

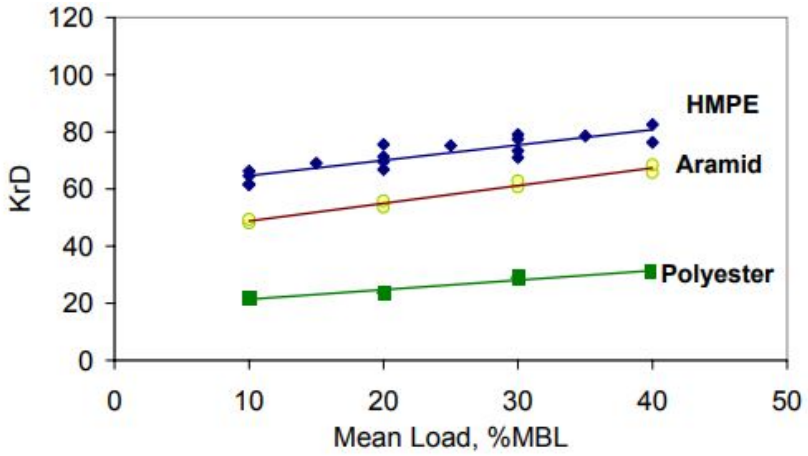

Figure 2.4: Influence of mean load on the stiffness parameter (Kr) for three different synthetic fiber ropes [47].

Raisutis et al. (2014) [48] showed that it is possible to detect defects in lines by looking at the attenuation of propagating waves. In this research, a multiwire steel rope was used and an artificial defect in the form of a cut was introduced to the rope. Furthermore, the effect of measuring propagating waves through the multiwire rope as a whole was compared to the propagation of waves through individual strands. The results are shown in figure 2.5.

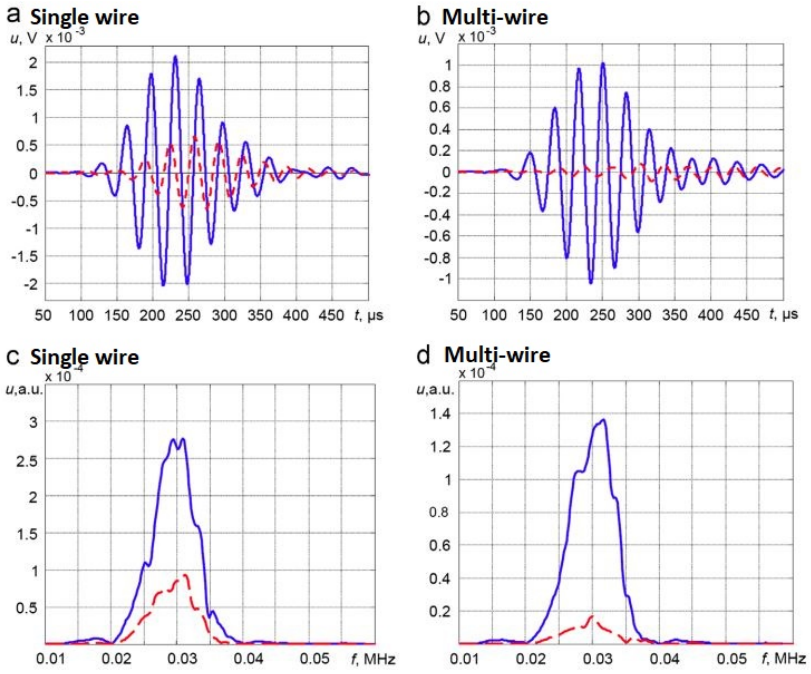

Figure 2.5: Waveforms and amplitude spectra of the flexural mode measured in defect-free (solid line) and defective regions (dashed line) in the case of the untwisted single strand (a and c) and the multi-wire rope (b and d)[48].

For simplicity, the single strand measurements (figure 2.5.a and 2.5.c) are considered. The solid blue lines indicate the measurements in the defect free strand and the red dashed line show the measurements for the strand with an artificial defect. There

is a clear drop in amplitude of the received signal in case there is a defect present. This indicates that it is possible to indicate whether a rope has been damaged based on ultrasonic guided wave measurements.

Vibration measurements
Finally, the load on a rope can be determined experimentally using vibration analysis. An example is a research by Mehrabi and Farhangdoust (2018) [23]. In this research, the tension in cable bridges has been determined using Laser Doppler Vibrometer (LDV) measurements. The LDV measurements were translated to vibrations of the cables which were naturally excited were possible or manually when necessary. The vibrations were translated to tension in the cables using formula 2.2.

$$T = \frac{4wf_n^2 L_e^2}{n^2 g} - \frac{(n\pi)^2 EI}{L_e^2} \quad (n = 1, 2, ...), \tag{2.2}$$

Previously acquired tension forces in the cables or predicted tension forces in the cables were then compared to actual tension forces which would lead to the conclusion on whether the cables were malfunctioning. A decreasing tension (or deviating tension from the expected) would indicate that a cable was damaged.

2.3. Chapter highlights

In the literature review, it was demonstrated that there are currently multiple structural integrity assessment techniques for the evaluation of synthetic mooring ropes. However, there is no technique that is capable of determining load on a synthetic mooring line using non-contact techniques. In fact, the only allowed inspection method currently is visual inspection which has many flaws and downsides. This justifies the need for an alternative non-contact structural integrity assessment technique.
It was concluded in section 2.2 that the tension can be calculated using vibration measurements when knowing the materials geometry and the stiffness. However, in the same section it was concluded that the stiffness is a function of load and increases under increasing load. Therefore, the stiffness is a variable and has to be determined in order to accurately determine the load. It was shown that the stiffness can be assessed using ultrasonic guided waves.

3

Methodology

3.1. General concept

In chapter 2 the different structural assessment techniques suitable for synthetic mooring lines were evaluated. Non-contact assessment of tension can be done using an LDV. However, equation 3.16 shows that the tension depends on multiple variables including the stiffness (E). Stiffness changes under load and should therefore be assessed. The stiffness will be assessed using non-contact ultrasonic guided wave (UGW) measurements. The methodology that will be used is thus based upon a combination of ultrasonic guided wave measurements and vibration measurements. The attenuation will be the result of the UGW measurements and vibrations will be the result of the LDV measurements.
As explained in chapter 2, a change in attenuation can indicate a number of things. First of all, a decrease in attenuation can indicate damage in the rope. Second, materials with higher densities will yield lower attenuation. Finally, higher stiffness yields a lower attenuation.

3.2. Theoretical concept

Ultrasonic guided waves

The wave equation for 1D waveguides will be derived [49]. The basis is the harmonic waveform.

$$u(x,t) = u_0 \cos(\omega t - kx) \tag{3.1}$$

where u is the amplitude at time t at position x, ω is the temporal frequency, k is the wave number and u_0 is half the peak-to-peak amplitude. Next, the second derivative with respect to time and position is calculated as

$$\frac{\partial^2 u}{\partial x^2} = -k^2 u_0 \cos(\omega t - kx) \tag{3.2}$$

$$\frac{\partial^2 u}{\partial t^2} = -\omega^2 u_0 \cos(\omega t - kx) \tag{3.3}$$

Rewriting equation 3.3 as $u_0 cos(\omega t - kx) = -\frac{1}{\omega^2}\frac{\partial^2 u}{\partial t^2}$ and substituting this result into equation 3.2 yields:

$$\frac{\partial^2 u}{\partial x^2} = \frac{k^2}{\omega^2}\frac{\partial^2 u}{\partial t^2} \tag{3.4}$$

Next, Newton's second law is considered.

$$F = m\frac{\partial v}{\partial t} \tag{3.5}$$

An ultrasonic wave travelling through a body as shown in figure 3.1 is assumed.

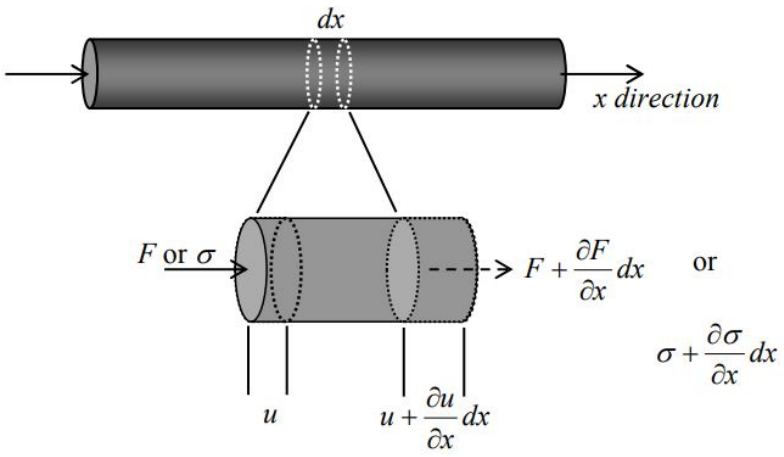

Figure 3.1: Ultrasonic longitudinal wave propagating in a rod [49].

Using figure 3.1, equation 3.5 can be rewritten as follows.

$$F = \left(\frac{\partial \sigma}{\partial x}dx\right)A \tag{3.6}$$

Where F is the force, σ is the stress and A is the cross-sectional area of the rod. Equating Newton's second law and equation 3.6 yields:

$$\left(\frac{\partial \sigma}{\partial x}dx\right)A = m\frac{\partial v}{\partial t} \tag{3.7}$$

Considering that $V = A \cdot dx$ and $v = \frac{\partial u_x}{\partial t}$, equation 3.7 can be rewritten as follows.

$$\frac{\partial \sigma}{\partial x} = \rho\frac{\partial^2 u_x}{\partial t^2} \tag{3.8}$$

Next, the first derivative of the stress-strain relation is considered.

$$\frac{\partial \sigma}{\partial x} = E\frac{\partial \varepsilon}{\partial x} \tag{3.9}$$

Substituting in equation 3.8 and expressing ϵ as function of displacement (u_x) yields:

$$E\frac{\partial^2 u_x}{\partial^2 x} = \rho\frac{\partial^2 u_x}{\partial t^2} \tag{3.10}$$

$$\frac{\partial^2 u_x}{\partial^2 x} = \frac{\rho}{E}\frac{\partial^2 u_x}{\partial t^2} \tag{3.11}$$

Next, the complex characteristic of a wave can be described as [50]

$$k^* = \frac{\omega}{c} + i\alpha \tag{3.12}$$

where k* is a complex wave number, c is the wave velocity, ω is the angular frequency, α is the attenuation coefficient, f is the frequency. The attenuation coefficient (α) can be determined as follows [51]:

$$\alpha = \frac{1}{d} ln\left(\frac{a}{a_o}\right) \tag{3.13}$$

where d is the distance between the reference location (x_{α_0}) and the considered location (x_α), a_0 is the amplitude of the signal at the reference location (x_{α_0}) and a is the amplitude of the signal at location x_α. According to formula 3.4 and 3.11, the wave number k* shown above can be related to material properties as follows:

$$\left(\frac{k^*}{\omega}\right)^2 = \frac{\rho}{E} \tag{3.14}$$

From this equation, it is clear that the wave parameters can be related to the material properties which shows the potential of the method. Assuming a constant rope density (ρ), the stiffness of the material (E) can be found from the attenuation and wave speed of the ultrasonic wave through the material.

Vibration analysis

Next, the derivation which forms the basis for the vibration analysis will be shown. The differential equation for motion considering flexural rigidity in the y-direction and the length of the cable in x-direction, assuming free decay is given as follows [52]:

$$\rho A\frac{\partial^2 y}{\partial t^2} - EI\frac{\partial^4 y}{\partial x^4} - T\frac{\partial^2 y}{\partial x^2} = 0 \tag{3.15}$$

Where ρ is the material density, A is the cross-sectional area of the test specimen, y is the coordinate of vertical direction due to vibration, t is the time in n seconds, EI is the bending stiffness of the rope (kNm^2), x is the coordinate in the longitudinal direction and T is the tension in the cable in kN. Assuming hinged boundary conditions on both sides gives [53]:

$$f_n = \frac{n}{2L}\sqrt{\frac{T}{m} + \left(\frac{n\pi}{L}\right)^2 \frac{EI}{m}} \quad (n = 1, 2, ...) \tag{3.16}$$

where f_n is the natural frequency at nth mode (Hz), n is the vibration mode, L is the effective length of the cable, T is the tension (kN), m is the mass per unit length of the vibrating test specimen and EI is the bending stiffness of the cable (kNm^2). Note that in the case of underwater analysis of mooring lines, the total mass per unit length consists of the structural mass per unit length of the specimen (m_s) and the added mass per unit length (m_a) [53]. The added mass can be calculated as $m_a = C_a \rho A$ where C_a is a constant depending on the geometry of the test specimen, ρ is the

density of water and A is the cross-sectional area of the submerged test specimen. According to DNV-RP-C205 [54], $C_a \approx 1$ for slender, circular rods. Equation 3.16 can be rewritten to find the tension as follows.

$$T = \frac{4 f_n^2 L^2 \left(m_s + m_a\right)}{n^2} - \frac{n^2 \pi^2 E I}{L^2} \tag{3.17}$$

It is evident from this equation that the tension depends not only on the frequency of vibration, but also on the stiffness. That is why the equation derived to calculate the stiffness using the ultrasonic guided waves will be used in combination with the equation derived for the vibration in order to find the tension.

3.3. Experimental concept

From equation 3.17, it is apparent that the natural frequency (f_n) and the stiffness (E) are the unknowns that should be determined in order to calculate the tension (T). Furthermore, from equations 3.14 and 3.13 it is apparent that the stiffness (E) can be calculated using the attenuation coefficient (α) of the guided wave travelling through the rope specimen. To find the unknowns, two measurements are performed. The natural frequency is assessed using modal analysis for which a Laser Doppler Vibrometer is used. The LDV measures the displacement and velocity of the vibrating rope the laser is pointing at. The rope is excited using an impact hammer which will cause vibration in the rope.
The stiffness of the specimen is determined by assessing the attenuation coefficient. The attenuation coefficient will be assessed using ultrasonic transducers which will have no contact with the rope. The goal is to find the attenuation of the signal when passing through the rope. However, the transducers are not in contact with the rope which causes a water gap between the transducers and the rope. The signal attenuates when passing through media which means that the signal attenuates when travelling through water too. If one transmitter and one receiver would be used, the water would have an influence on the results as the attenuation would be the sum of the attenuation in water and attenuation in the rope. In order to account for this, a second receiver is added to the setup.
A schematic overview of the test setup may be found in figure 3.2. The figure shows both the LDV and UGW setup including the required systems, as well as the placement of the test specimen and the direction of the applied load.

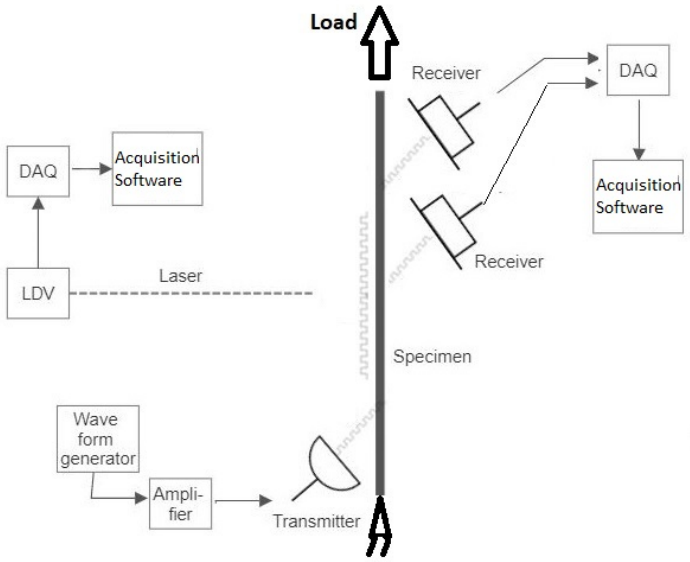

Figure 3.2: Schematic overview of the test setup.

It is important that both assessments are performed under the same load. Therefore, the tests shall be performed in load steps in order to get accurate results. This means that a load shall be put on the specimen and this load shall be held until the guided wave measurements and vibration measurements have been performed.
The tests will be performed at 5 different loads, namely 1kN, 2kN, 3kN, 4kN and 5kN. This is a relatively low load which is due to a combination of factors including the maximum allowable load of the shackles connecting the rope to the testing machine and the need to avoid slip of the knots in the rope. The Minimum Breaking Load (MBL) of the rope is 80kN which means that the maximum applied load (5kN) is approximately 6% MBL.

3.4. Data processing

This section will cover the data processing approach. The data processing consists of two parts, the data processing of the UGW measurements and the data processing of the LDV measurements.

Ultrasonic guided wave measurements

The ultrasonic guided waves are generated by a waveform generator. Due to the fact that the transmitter and receivers are not in contact with the rope, the transmitted pulse will travel to the receivers through different mediums. Part of the transmitted pulse travels through the rope and another part of the pulse will travel through water. Due to the fact that the wave speed in water is lower than the wave speed in HMPE, the wave travelling through water will reach the receiver later than the wave travelling through the rope. In figure 3.3, an example of a typical waveform received by one receiver in this configuration can be found. Note that this is an example graph and the y-axis (received signal strength) and x-axis (time) should not be considered accurate values. In this example graph, the green encircled waveform is the wave part travelling

through the rope and the red encircled waveform is the wave part travelling through water.

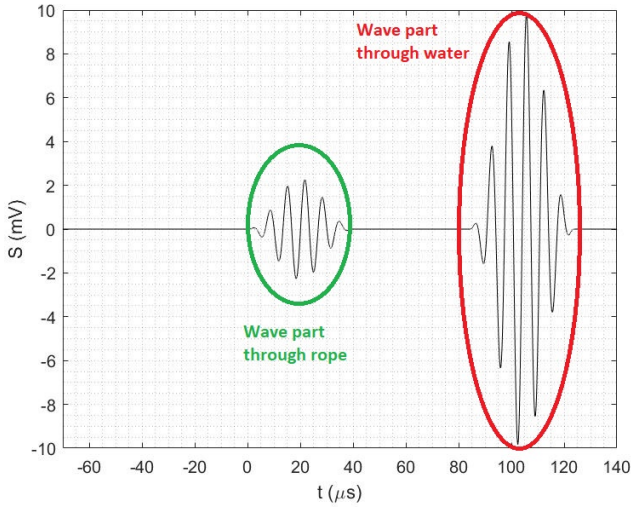

Figure 3.3: Example of a typical waveform received by a receiver in this configuration.

The attenuation is defined as the reduction of amplitude of a signal. Due to attenuation, the amplitude of the received signal decreases over longer distances which is also apparent from equation 3.13.

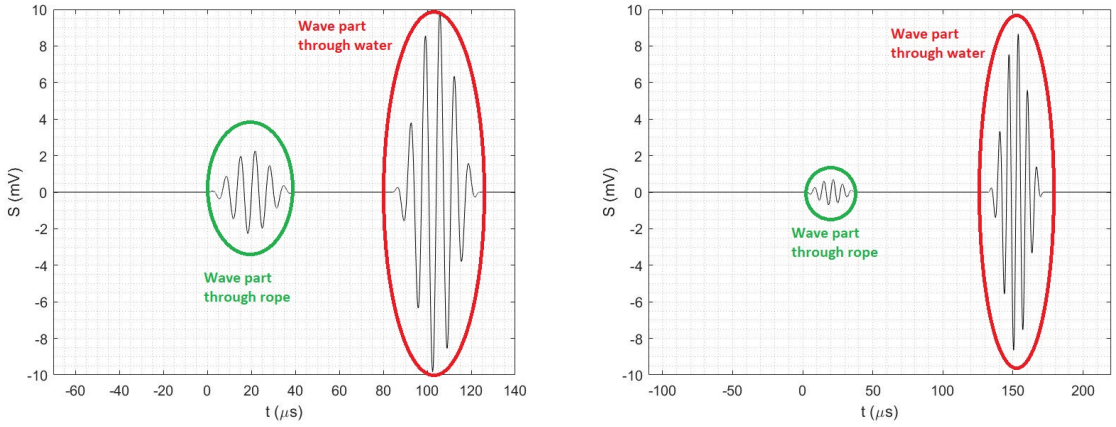

(a) Example of typical waveform received by the lower receiver (closest to transmitter).

(b) Example of typical waveform received by the upper receiver (furthest away from transmitter).

Figure 3.4: Examples of typical waveforms at two different receivers.

The effect of decreasing amplitude due to attenuation can be seen in figure 3.4. In figure 3.4a, one can see a typical waveform at the lower receiver while in figure 3.4b, one can see a typical waveform at the upper receiver. These figures show how the amplitude of the wave part travelling through the rope decreases with increasing distance. This is the attenuation effect which is used in formula 3.13 to calculate the stiffness as in formula 3.14.
In order to find the amplitude of the wave part of interest, the Hilbert transform of the signal is determined. Figure 3.5 shows an example of the Hilbert transform.

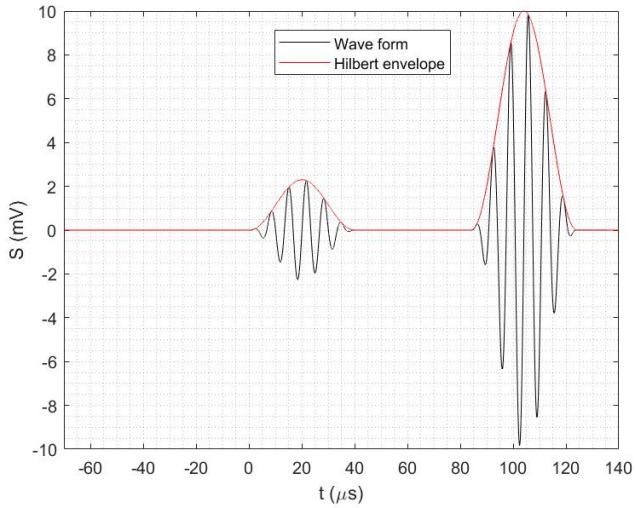

Figure 3.5: Example of a typical waveform received by a receiver in this configuration including the Hilbert transform.

With the Hilbert transform, the maximum amplitude of the wave part of interest can be determined as shown in figure 3.6. The maximum value is the input value (a) in formula 3.13. From the same formula it is apparent that this input value (a) has to be compared to the reference value (a_0).

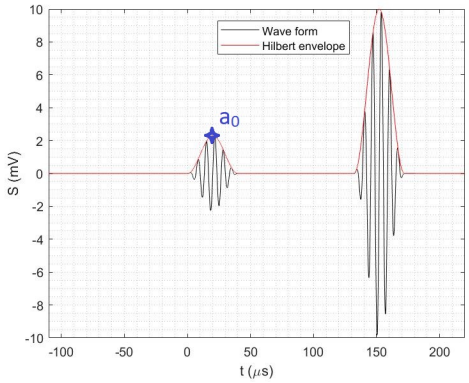

(a) Example of typical waveform received by the lower receiver (closest to transmitter) including Hilbert transform. The cross (a_0) indicates the maximum of the Hilbert transform of the wave part of interest.

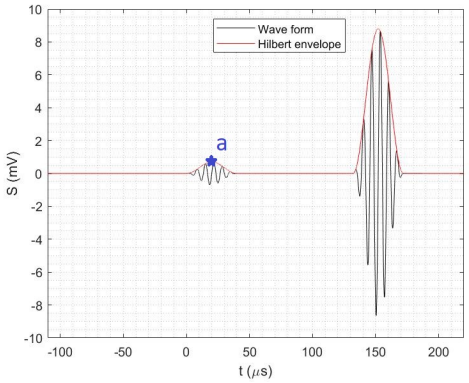

(b) Example of typical waveform received by the upper receiver (furthest away from transmitter) including Hilbert transform. The star (a) indicates the maximum of the Hilbert transform of the wave part of interest.

Figure 3.6: Examples of typical waveforms at two different receivers.

The reference value is usually the maximum amplitude of the Hilbert transform of the pulse sent from the transmitter. However, in this case there is no contact between the rope and the transmitter and receivers which means there is a water gap. In water, the wave experiences attenuation as well. This means that the maximum of the Hilbert transform of the sent pulse can not be used as a reference value to determine the attenuation of the rope. Instead, the maximum of the Hilbert transform of the wave travelling through the rope picked up by the lower receiver will be used as reference value (a_0) and the maximum of the Hilbert transform of the wave travelling through the

rope picked up by the upper receiver will be used as input (a). In this way, the effect of the attenuation in water is cut out.

Vibration measurements

The vibration of the rope is measured during the experiment using the LDV. During the measurement, the rope is hit multiple times using the impact hammer. One hit of the impact hammer yields a result measured by the LDV as shown in figure 3.7. The values for time and amplitude are representable for actual test conditions and are given in seconds and volts respectively.

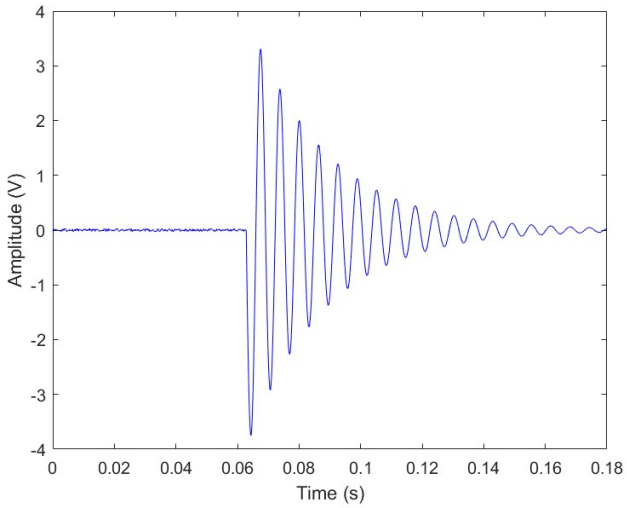

Figure 3.7: Example of the LDV result after one hit with the impact hammer.

The resulting graph is the displacement or velocity. Both the displacement and velocity will yield the same result as they can both be translated to the frequency of vibration. In order to find the frequency of vibration, the Fast Fourier Transform can be used. The Fast Fourier Transform yields a graph as shown in figure 3.8. The graph shows the frequency content of the example LDV result from figure 3.7. The curve shows a peak at approximately 95Hz indicating that the frequency of vibration is 95Hz.

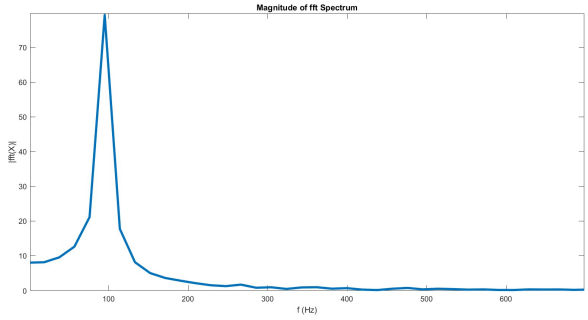

Figure 3.8: Fast Fourier Transform of the example LDV result in figure 3.7.

This result, in combination with the stiffness determined using the UGW results, can be used to determine the tension in the rope using equation 3.17.

3.5. Hypothesis

The hypothesis is that the attenuation of the ultrasonic guided waves will decrease for higher load values. This is due to the fact that a higher load translates to an increase in stiffness of the HMPE test specimen and an increased stiffness leads to a lower attenuation. Based on the guided wave attenuation (α), the increase in stiffness can be determined. In order to verify this result, a reference (literature) value for the stiffness will be used.
Furthermore, the hypothesis is that the natural frequency of vibration increases when a higher load value is applied to the specimen. According to formula 3.16, the increase in frequency should scale with the root of the applied load.

3.6. Chapter highlights

In this chapter, the proposed methodology is presented. The theoretical concept presented in section 3.2 shows the derivation of the formulae used for the determination of the stiffness and the tension using ultrasonic guided wave measurements and vibration analysis. The experimental concept presented in section 3.3 shows how the attenuation and the vibration are determined using ultrasonic transducers and a Laser Doppler Vibrometer respectively. It was determined that the tests are conducted at 1, 2, 3, 4 and 5 kN to put the proposed methodology to the test.
Next, section 3.4 showed how the recorded data is processed in order to find the attenuation and the natural frequencies. It is expected that the attenuation of the ultrasonic guided waves will decrease for higher loads. Furthermore, it is expected that the natural frequency increases with increasing axial load on the test specimen.

4

Experiments

4.1. Test specimen

The collaboration partner Avient provided 100 meters of DM20, HMPE rope. The DM20 rope is shown in figure 4.1 and general information about the rope that has been used during the experiment can be found in table 4.1.

Figure 4.1: Rope specimen provided by Avient.

Table 4.1: General information about test specimen

Number of strands (-)	10
Diameter (mm)	10
Initial length (mm)	471

The properties of DM20 are shown in table 4.2.

Table 4.2: Selected properties of DM20 [9].

	DM20
Density (g/cm^3)	0.98
Melting Point (°C)	148
Modulus (N/tex)	96
Tenacity (mN/tex)	3200
Break Extension (%)	3.6
Moisture (%)	0

Note that the modulus and tenacity are expressed in N/tex and mN/tex respectively. These units are often used when referring to synthetic fiber ropes as it is more convenient to express the modulus and break strength (tenacity) in terms of linear density due to the fact that it is a woven material [55]. Tex is the unit for linear density of the fiber and has units of g/km. This means that the modulus and tenacity (in N/tex and mN/tex respectively) are provided in units of breaking strength per linear density. For reference, the modulus and tenacity can be translated to units of MPa by multiplying the modulus and tenacity (in N/tex) by $1 \cdot 10^6$ and ρ. For DM20, this yields a modulus of $94GPa$ and a breaking strength of $3.1GPa$.

4.2. Test setup

This section provides an overview of the test setup, as used during the experiments. The actual test setup in the lab may be found in figure 4.2.

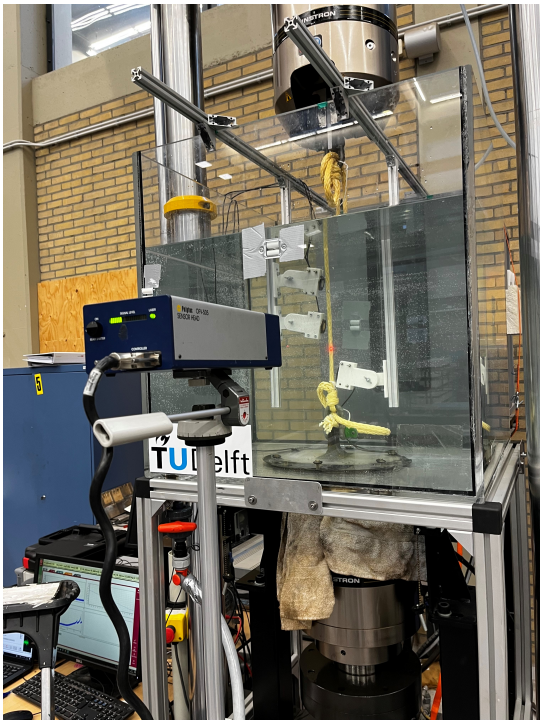

Figure 4.2: Test setup in the lab.

As may be seen from the figure, there is a small gap between the transmitter/re-

ceivers and the rope. This gap is 5mm for all three transducers. The vertical distance between every transducer is 100mm, see figure 4.3. Furthermore, the LDV is placed outside the water tank and it is thus measuring through the plexiglass and the water. The water inside the tank is artificial sea water. A total of 5.5kg of salt is added to 220l of water in order to get a density of approximately 1025kg/m^3 which is representative for sea water.
To connect the test specimen to the testing machine, two shackles have been used. The test specimen is tied to the shackles using so called scaffold knots.

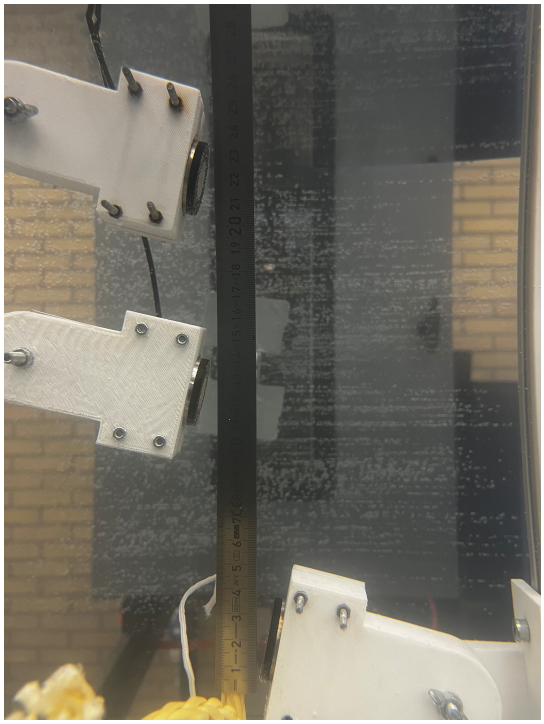

Figure 4.3: Vertical distance between transducers.

For these tests, the Instron 8854 axial – torsion testing machine is used. Table 4.3 shows the specifications of the testing machine. F_n denotes the machines axial load capacity, $\mathbf{u}$ the axial actuator stroke, M_t the torque capacity and α the rotary stroke.

Table 4.3: Specifications of the Instron 8854 axial - torsion testing machine

F_n	$\mathbf{u}$	M_t	α
$\pm 250[kN]$	$\pm 50[mm]$	$\pm 2000[Nm]$	$\pm 45[deg]$

Due to the fact that (scaffold) knots are used as connection to the shackles in the system, the rope experiences some unwanted slip. Furthermore, the material is viscoelastic. This means that the material relaxes when a constant displacement is applied to the material and is held there. As a result, the load will decrease when the displacement is held constant which is fundamentally different from a pure elastic material such as steel. For the tests, it is necessary to keep a constant load throughout the individual measurements and therefore, the load control option provided by the Instron testing machine software is used.

4.3. Data acquisition

The ultrasonic transducers and the LDV use different hardware for data acquisition. Figure 4.4 shows the data acquisition system used for the UGW measurements.

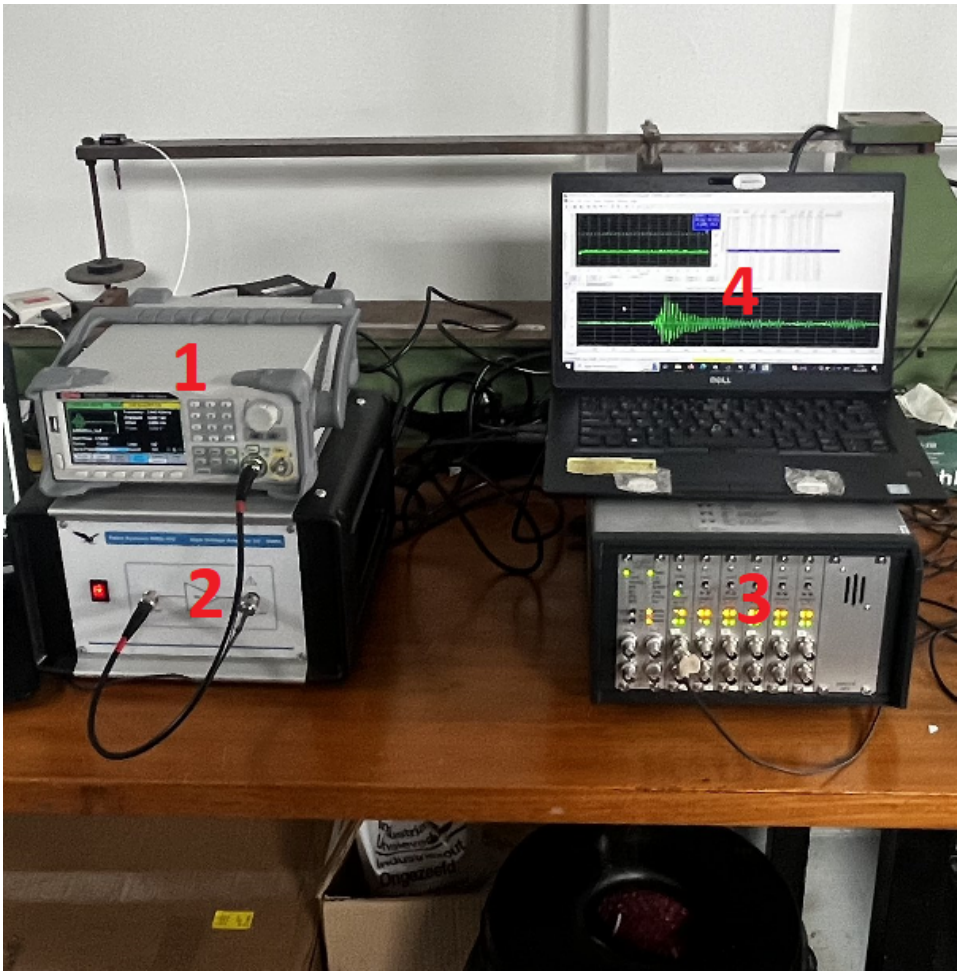

Figure 4.4: Data acquisition system of the ultrasonic transducers.

The figure shows the waveform generator (1), the high voltage amplifier (2), the data acquisition system (3) and the data acquisition laptop with DAQ software (4). The waveform generator is the type RS PRO RSDG1032X [56]. The waveform generator is connected to the high voltage amplifier, which is a Falco WMA-300 [57]. Connected to the high voltage amplifier is a transducer that will act as transmitter. The transducer is a Vallen VS150-WIC-V01 [58]. The two receivers are the same Vallen VS150-WIC-V01 transducers as this type can both transmit and receive signals. The two receivers are connected to the data acquisition system which is a Vallen AMSY-6 MB6 [59].

Figure 4.5 shows the data acquisition system used for the LDV.

Figure 4.5: Data acquisition system of the LDV.

The figure shows the LDV controller (1), the oscilloscope (2) and the impact hammer (3). The LDV sensor head is a Polytec OFV-505 [60]. The sensor head is connected to the LDV controller (type OFV 2200 [61]). To transfer the velocity output of the LDV controller, an oscilloscope is connected to the LDV controller. The oscilloscope that is used is a Micsig TO202A [62]. Furthermore, the impact hammer, which is a type DJB IH/02 produced by DJB Instruments [63], is connected to the oscilloscope as well. Therefore, the oscilloscope measures the pulse of the impact hammer due to hitting the rope and the velocity component measured by the LDV. The data measured by the LDV is transferred to a flash drive after which the data can be processed using Excel and Matlab.

4.3.1. Settings

This section will discuss the settings of the waveform generator and the data acquisition systems used for the UGW measurements and the vibration measurements.

Waveform generator

The transmitted waveforms used during the UGW experiments are narrow-banded Hanning-windowed sinusoidal pulses [64]. Waveforms with different center frequencies (50, 100, 150, 200, 250 and 300 kHz) have been used during trial experiments. It was noticed that at 150 kHz, the resulting wave part travelling through the rope had the highest amplitude compared to other center frequencies which makes the wave part of interest best distinguishable from noise. Therefore, a transmitted waveform with a center frequency of 150 kHz was used during the experiments. The characteristics of the transmitted waveform are shown in table 4.4.

Table 4.4: Settings of transmitted waveform

Center frequency (kHz)	Number of peaks (-)	Burst Interval (s)	Amplitude (V_{pp})
150	6	1	10

The characteristics described in table 4.4 produce a waveform as shown in figure 4.6.

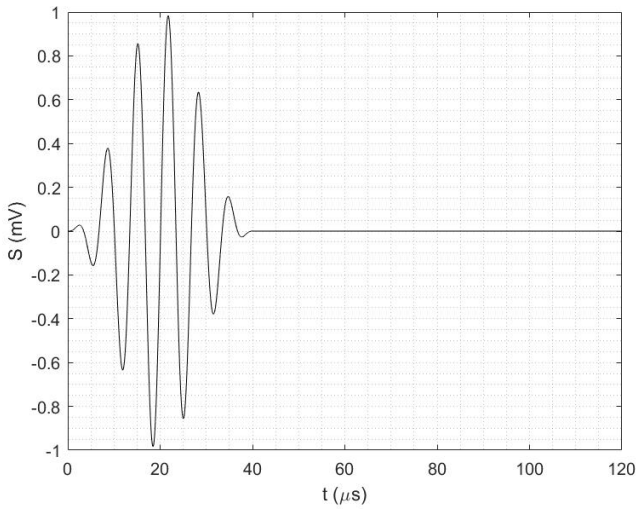

Figure 4.6: waveform transmitted by the transmitter during the experiments.

Data acquisition settings for the UGW measurements

The data acquisition setting used for the UGW measurements are shown in table 4.5. Note that the settings are for the receivers. The transmitted waveform is recorded too, with the difference being that the threshold is 100dB rather than 30.1dB.

Table 4.5: Data acquisition settings for the UGW measurements.

Sample rate (MHz)	Samples per set (-)	Duration discrete time (μs)	Rearm time (μs)	Threshold (dB)	Pre-trigger (μs)	Post-duration (μs)	Filter (kHz)
2.5	4096	250	250	30.1	400	1250	20-500

Data acquisition settings for the vibration measurements

The data acquisition settings used for the vibration measurements are shown in table 4.6. In this case, record length is the amount of data points the software can store for one individual measurement.

Table 4.6: Data acquisition settings for the vibration measurements.

Sampling frequency (kHz)	Record length (-)
250	45000

Please note that the record length is set at 45000 for this particular oscilloscope. The sampling frequency is the same for all measurements which means that each individual measurement contains 0.18 seconds of vibration data.

5

Results

5.1. Laser Doppler Vibrometer measurements

This section will show the results from the Laser Doppler Vibrometer measurements. The tests are performed according to the methodology described in chapter 3. The LDV response graph at 5kN is given in figure 5.1a and the corresponding frequency domain (showing a frequency of 216.67Hz) is given in figure 5.1b. Please note that the frequency of (free) vibration is analysed rather than producing a Frequency Response Function using the impact hammer.

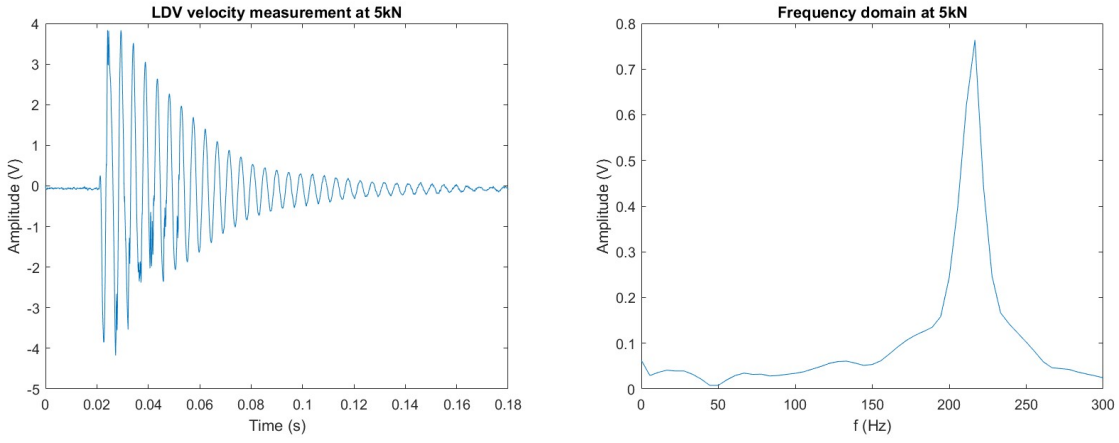

(a) LDV response graph at 5kN.

(b) Frequency domain of the response.

Figure 5.1: LDV response graph and frequency domain of this response.

As mentioned in chapter 4, 5 hits per load are performed and thus there are 5 frequencies per load to compare. Figure 5.2 shows the experimental results measured by the LDV for the 5 applied loads.

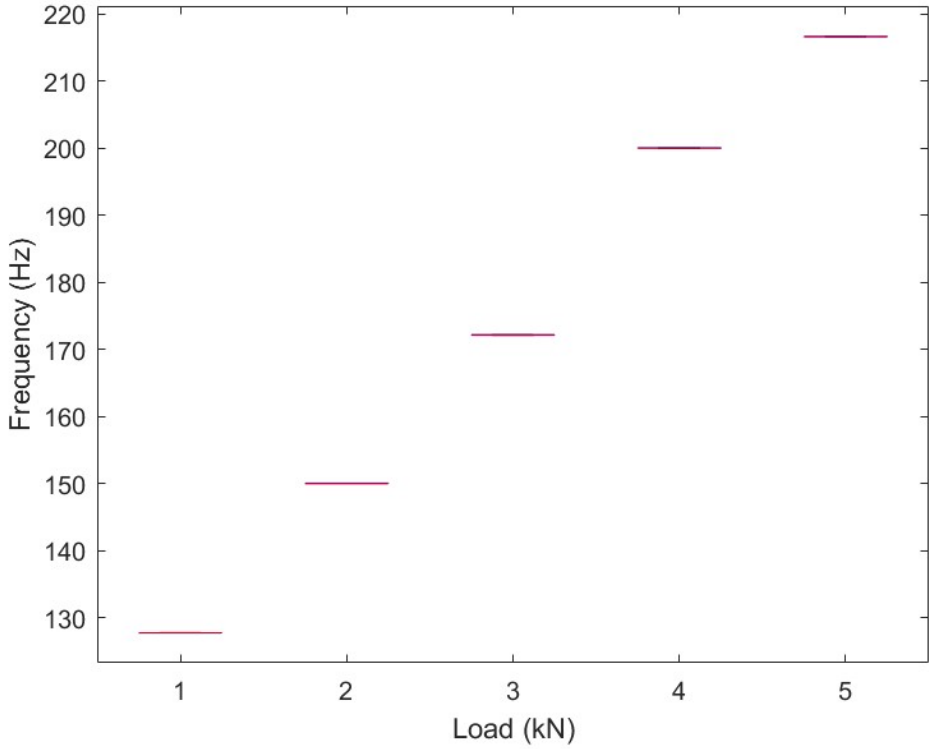

Figure 5.2: Experimental frequency of vibration measured for all applied loads.

The results are shown in the form of a boxplot. The boxplots show that the spread in the result is small for all load levels (in the range of $\pm 0.1Hz$ for all load levels). For increasing loads, a higher frequency is measured which is in line with the hypothesis. According to the hypothesis, the frequency increases with approximately the root of the load ($f \propto \sqrt{T}$). This is visualised in figure 5.3. This graph shows the theoretical frequencies and the measured frequencies to check whether the measured frequencies correspond with the expected frequencies. From the figure it is clear that the measured frequencies are in the range of the values they should theoretically be. The deviations are expected to be due to assumptions made in the derivation of the formula for the frequency (formula 3.16) which was used to calculate the expected frequencies. In the derivation, it is assumed that the test specimen is either fully in air, or fully submerged in water. In this case however, part of the test specimen is submerged in water and a small part of it is in air. Approximately 70% of the test specimen is submerged in water during the experiments. Therefore, a part of the rope is experiencing the damping effect of the surrounding water while another part does not experience this damping. Therefore, the derivation is inaccurate as it is oversimplified in this case. The measured values are however close enough to the theoretical values to proceed with this approach.

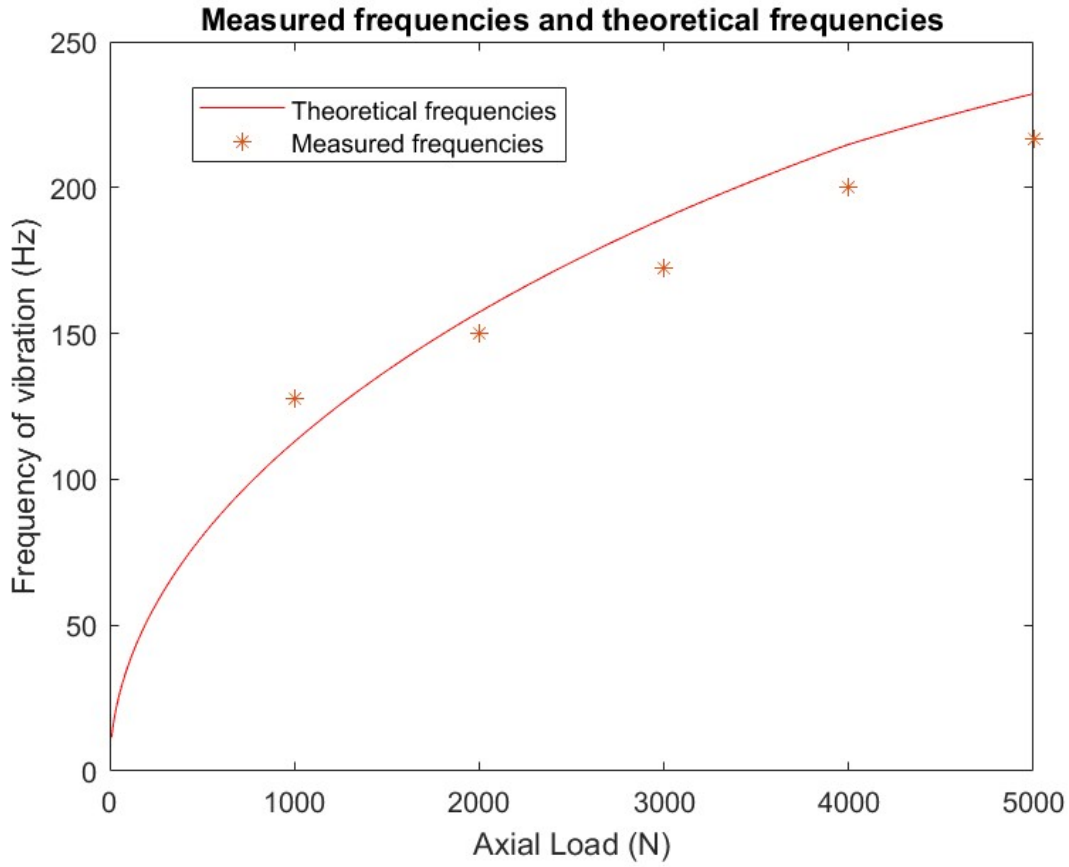

Figure 5.3: Experimental frequency of vibration measured for all applied loads and theoretic values.

5.2. Ultrasonic guided wave measurements

This section shows the UGW results. The tests are performed according to the methodology described in chapter 3. The ultrasonic measurements at a load of 5kN are shown in figure 5.4. In red encircled are the wave parts travelling through water. In green encircled are the wave parts travelling through the rope. The upper figure shows the pulse sent from the transmitter at t=400μs. The middle figure shows the ultrasonic waves received by the lower receiver. Finally, the lower figure shows the ultrasonic waves received by the upper receiver. The results for the lower and upper receiver are time shifted with respect to the pulse sent by the transmitter. For the receivers, alongside the waveforms, the Hilbert transforms are plotted. As explained in chapter 3, the maximum amplitudes of the Hilbert transform are used to determine the attenuation.

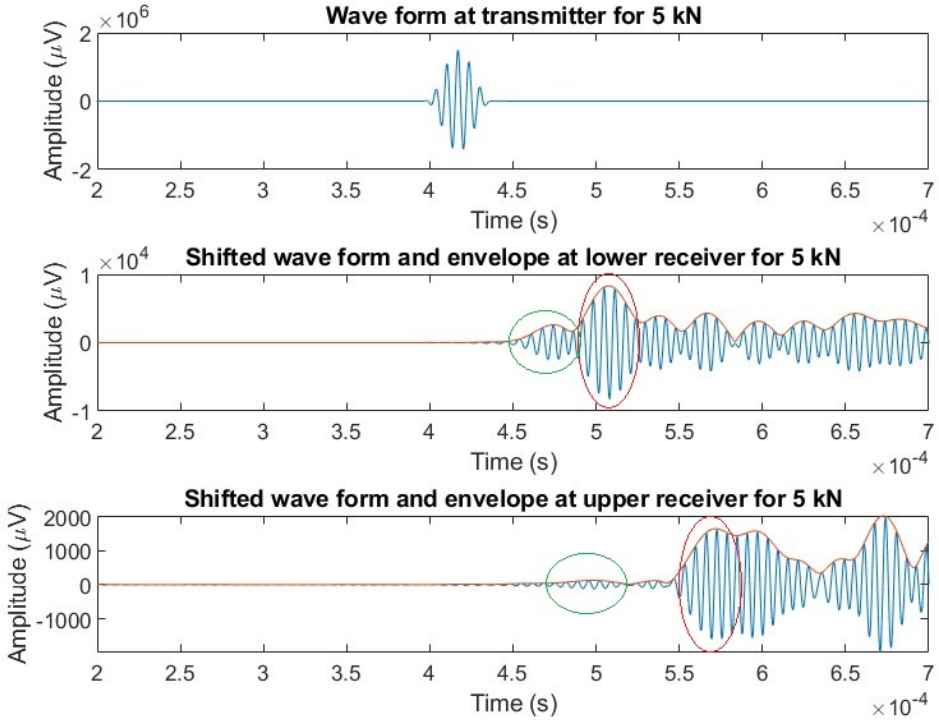

Figure 5.4: Ultrasonic measurements at 5kN.

At every steady load (1, 2, 3, 4 and 5kN), the measurements are performed for at least one minute generating at least 60 data points. For every measurement, the maximum of the Hilbert transform at the wave part of interest (the wave through the rope) is determined. The resulting maximum amplitudes can be presented in the form of a boxplot. The results for the lower receiver are presented in figure 5.5 and the results for the upper receiver are presented in figure 5.6.

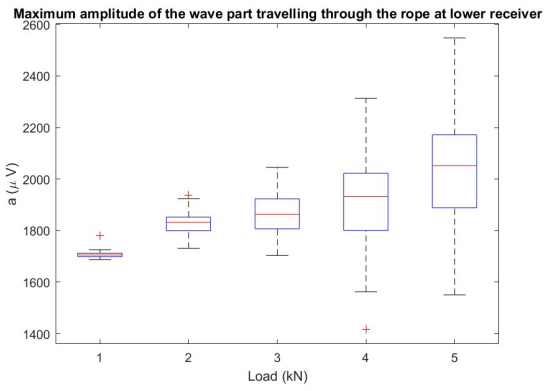

Figure 5.5: Amplitude (a_0) of the wave part through the rope for all load levels at the lower receiver.

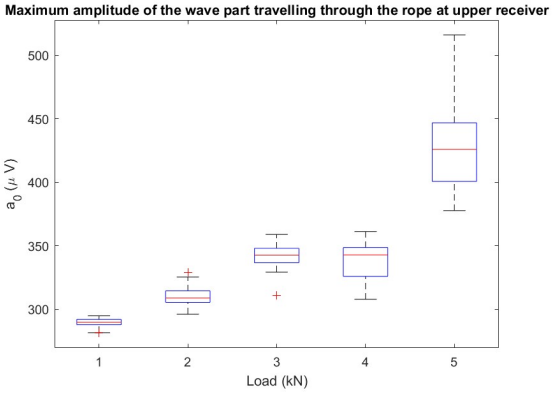

Figure 5.6: Amplitude (a) of the wave part through the rope for all load levels at the upper receiver.

According to formula 3.13, the fraction $\frac{a}{a_0}$ determines the attenuation coefficient (α). The results for this fraction are shown in figure 5.7 for all load levels.

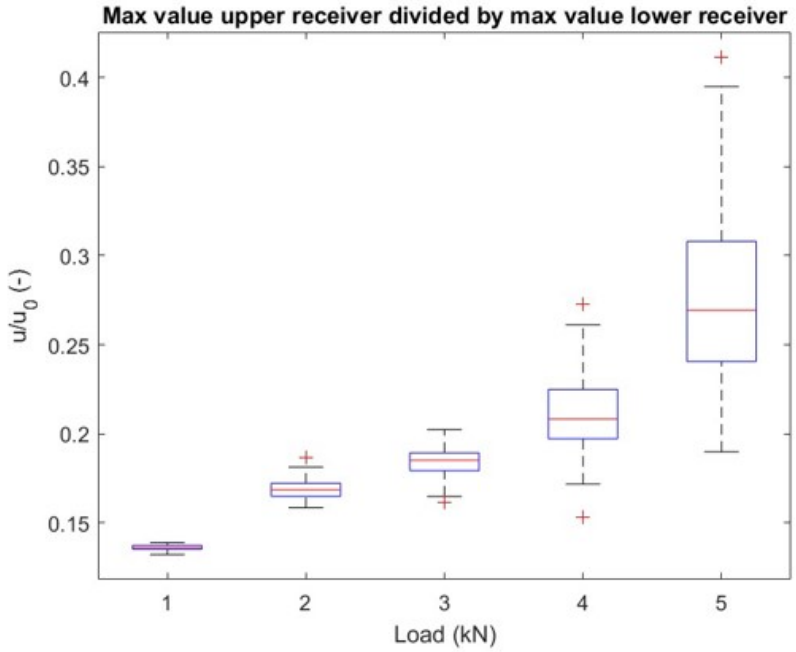

Figure 5.7: a/a_0 for all load levels.

The results show an increasing trend for higher load values indicating a higher attenuation coefficient. For the stiffness calculations, the median values of the $\frac{a}{a_0}$ results are used. The medians are given in table 5.1.

Table 5.1: Median results of the $\frac{a}{a_0}$ fraction for all applied loads.

Applied load (kN)	$\frac{a}{a_0}$ **(-)**
1	0.136
2	0.169
3	0.185
4	0.208
5	0.269

5.3. Stiffness assessment

The results from the ultrasonic guided wave measurements can be converted to stiffness using the results from figure 5.7 according to formula 3.14. Recall that this formula is given as follows.

$$\left(\frac{k^*}{\omega}\right)^2 = \frac{\rho}{E} \tag{5.1}$$

where,

$$k^* = \frac{\omega}{c} + i\alpha \tag{5.2}$$

and,

$$\alpha = \frac{1}{d} ln\left(\frac{a}{a_o}\right) \tag{5.3}$$

All variables except E and c are known. Usually, UGW measurements can be used to determine the wave speed of waves travelling through the specimen by using the time of arrival of wave parts of interest. However, due to inaccuracies in the experiments, the wave speed can not be calculated with the desired accuracy. Therefore, it is chosen to take the reference value of longitudinal waves in HMPE material which is approximately $10.000\frac{m}{s}$ [65]. With all variables in equation 5.1 known, the stiffness (E) can be calculated. Table 5.2 shows the calculated stiffness for all applied loads according to the obtained values for the attenuation. Note that the values are presented as complex numbers. This is the viscoelastic nature of the material where the real part is the storage modulus and the imaginary part is the loss modulus.

Table 5.2: Stiffness calculated from experimental attenuation values for all applied loads.

Applied Load (kN)	Complex Stiffness (GPa)
1	85.8 + 38.0i
2	88.1 + 34.5i
3	89.1 + 32.9i
4	90.2 + 30.9i
5	92.5 + 26.2i

5.4. Load assessment

Combining the stiffness calculated in the previous section and the measured frequencies, formula 3.17 can be used to determine the calculated tension in the rope. Recall that formula 3.17 is given as follows.

$$T = \frac{4f_n^2 L_e^2 (m_s + m_a)}{n^2} - \frac{(n\pi)^2 EI}{L_e^2} \quad (n = 1, 2, ...), \tag{5.4}$$

All variables are now known except the length (L_e) of the rope since the length is changing due to the slipping of the knots. The length of the rope was measured at the start of the measurement at 1kN and was measured to be 471mm. Using the Instron measurements of the displacement, the lengths of the rope at all individual load levels can be determined. The different lengths at different load levels are shown in table 5.3.

Table 5.3: Lengths of the rope at the applied loads, starting from the moment the LDV measurements started.

Applied Load (kN)	Length (mm)
1	471
2	478
3	486
4	495
5	512

It is assumed that the biggest contribution to the vibration is the fundamental mode (n=1). For the rest, the weight and moment of inertia are material properties/geometries and are known. Furthermore, the stiffness in table 5.2 is presented as a complex number. This relates to the fact that the test specimen is a viscoelastic material. The real part of the complex stiffness is the storage modulus which relates to the materials ability to store energy elastically. On the other hand, the imaginary part is the loss modulus which relates to the materials ability to dissipate stress through heat [66]. Both the storage modulus and the loss modulus contribute to the overall stress in the material and therefore, the absolute value of the complex stiffness is used in order to calculate the tension using formula 3.17. This leads to a calculated load as found in table 5.4.

Table 5.4: Loads (kN) calculated from the combination of the stiffness and the frequency.

Actual Applied Load (kN)	Calculated Load (kN)
1	1.3
2	1.9
3	2.5
4	3.5
5	4.4

5.5. Discussion of the results

5.5.1. Discussion of the LDV results

The LDV results show small variation between different measurements for every load. The variation between frequency measurements at the same load level are in the order of $\pm 0.1 Hz$ which is a variation of less than 0.1% of the median. Furthermore, a trend of increasing frequency is visible when the tension is increased. This is in line with the hypothesis and is intuitively correct. It is known from simple string vibration theory that the frequency is a function of the root of the tension in the string (assuming no stiffness and inertia of the string). The same phenomenon is apparent from equation 3.17 where the stiffness and inertia of the string is included.

5.5.2. Discussion of the UGW results

The results of the UGW measurements, shown in figure 5.7, are in accordance with the hypothesis which states that increasing stiffness yields a lower attenuation. As shown by Davies et al. (2002) [47], the stiffness of HMPE fiber ropes increase when the load increases. This means that higher loads yield lower attenuation and thus more energy of the wave received by the receivers. This effect is visible in figure 5.7 as the fraction of the wave part travelling through the rope received by lower and upper receiver increases for higher loads. The individual results for the lower and upper receiver (figure 5.5 and 5.6) show the same increasing trend.
It is noticeable in the boxplot that the variation in results increases for higher load values. For example, for 1kN, the difference between the 75th percentile and the median is only 0.7% while for 5kN the difference between the 75th percentile and the median is 10.9%. Different possible explanations for this effect are explored. Possible

explanations are divided into internal and external effects. The internal effect possibly causing this effect is the changing loss modulus of the stiffness. The external effects possibly causing this effect are changes in properties of the water, vibrations in the test setup, increased scatter of ultrasonic guided waves due to increasing stiffness of the test specimen and changing surface area geometry faced by the transducers due to slip of the test specimen. First, it needs to be determined whether it is an effect that is related to an internal or external source. To determine this, the wave velocity of the part of the wave travelling through water is determined and is shown in figure 5.8. The wave velocity of the wave travelling through water is calculated by dividing the distance between the transmitter and the lower receiver by the time difference between the moment the pulse is transmitted and the pulse is received by the lower receiver. The time picking is done according to the methodology described in chapter 3.4, meaning that the maximum amplitude of the Hilbert transform of the diagnostic wave and the wave travelling through water is determined and the time value of this maximum amplitude is picked. The time value of the maximum amplitude of the diagnostic wave is defined as t_0 and the time value of the maximum amplitude of the wave travelling through water received by the lower receiver is defined as t_1. The distance between the transmitter and the lower receiver is defined as d_{t-lr}. The wave velocity of the wave through water is therefore defined as

$$c_w = \frac{d_{t-lr}}{t_1 - t_0} \tag{5.5}$$

The wave velocity through water shows the same increasing scatter in the results for higher load values. This leads to the conclusion that the increasing scatter in results for increasing load is related to an external effect since the wave velocity through water would not show the same increased scatter for higher load values if it was purely related to internal effects of the test specimen.

Therefore, the possible explanations related to external effects (changing water properties, vibrations in the test setup, increased scattering of the waves and changing surface area geometry faced by the transducers due to slip of the test specimen) are evaluated. It is known that an increase in temperature of the water will lead to an increased speed of sound through water [67]. Looking at the extreme case of 5kN in figure 5.8, it can be seen that the median is at 1482m/s which agrees with the value found by Kumar, Pathak and Dass (2016) [67] at room temperature. The extreme value (outlier) at 5kN is 1548m/s which, according to [67] would mean that the water has reached a temperature of approximately 70 degrees Celsius. It is highly unlikely that this has happened during the experiment and this theory is thus rejected.

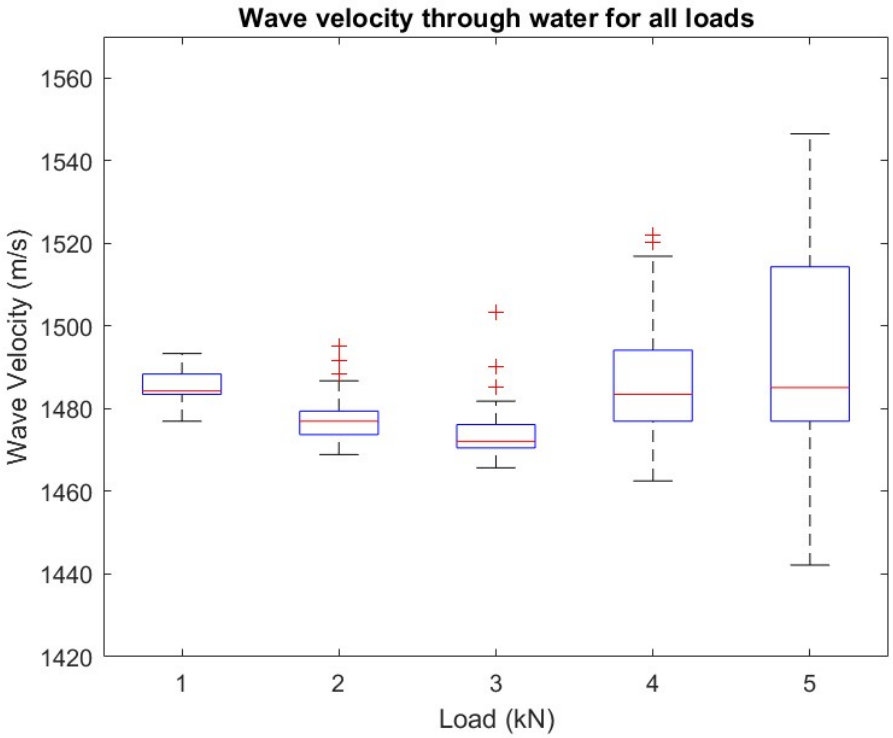

Figure 5.8: Wave velocity through water for all loads.

The system is likely to experience some vibration due to the force being exerted by the Instron machine. Due to this vibration, a swinging motion of the transducers could take place due to the way they are suspended in the tank. In order to evaluate this theory, the time of arrival of the wave package travelling through water is used which is shown in figure 5.9. The time of arrival is calculated by defining the maximum amplitude of the Hilbert transform as described in chapter 3.4. The time of arrival is the difference between the time value of the maximum of the Hilbert transform of the wave travelling through water received by the lower receiver and the time value of the maximum of the Hilbert transform of the transmitted wave. The outliers are evaluated for the extreme condition (5kN). The lower outlier is $87\mu s$ and the higher outlier is $93\mu s$ yielding a difference of $6\mu s$ between the two extreme values. Assuming a constant wave velocity of sound in water of 1482m/s, it is calculated that a difference of 6 μs for the time of arrival would yield a required variation in distance equal to 8.9mm. This means that the transducers would have to swing back and forth with a maximum amplitude of approximately half a centimeter. It is assumed that this would have been noticeable during the experiment. However, no such observation has been made. Therefore, this theory is rejected.

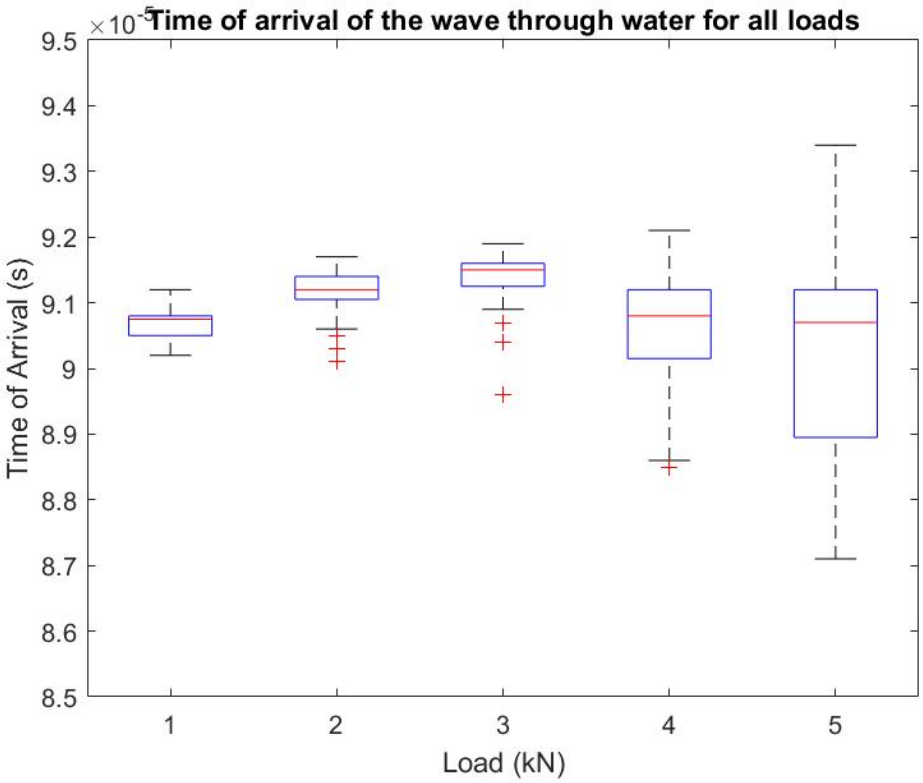

Figure 5.9: Time of arrival of waves through water for all loads.

It should be taken into consideration that the knots were experiencing slip during the experiment. The slipping is visualised in figures 5.10 and 5.11. The figures show the displacement of the moving loading head of the Instron machine for the lowest applied load (1kN) and the highest applied load (5kN). The figures show that over 30 seconds during testing, the displacement (and thus the slip) at 1kN is approximately 0.05mm while at 5kN, the displacement is approximately 0.45mm. This indicates that at higher loads, the slip is increasing. This could have affected the results of the UGW (shown in figure 5.5 and 5.6) since due to the slip, the rope is constantly (slightly) moving in the longitudinal direction. The test specimen is woven from strands which means that the outer surface of the rope is not smooth. The transducers are fixed in their position with respect to the tank which means that when the rope is slipping, the surface area of the rope that the transducers are facing is changing continuously. This may have an influence on the results as a changing geometry of the surface the transducers are facing can reflect the transmitted ultrasonic guided waves differently. This could explain the larger spread in resulting amplitudes of the ultrasonic guided waves travelling through the test specimen for higher load values, which can be observed in figure 5.5 and 5.6. With more slip, the outer surface of the test specimen that the transducers are facing is changing more rapidly which means the reflection of waves is changing more at higher loads.

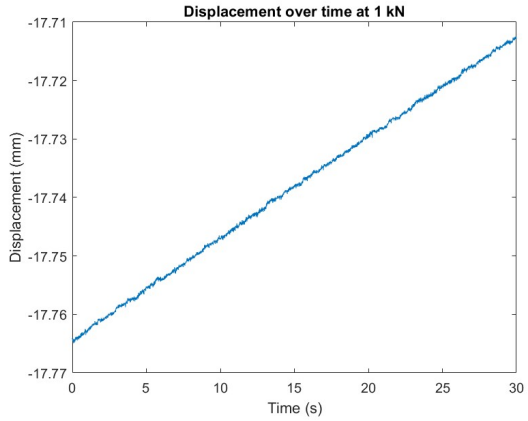

Figure 5.10: Displacement of the loading head of the Instron machine over time at 1 kN.

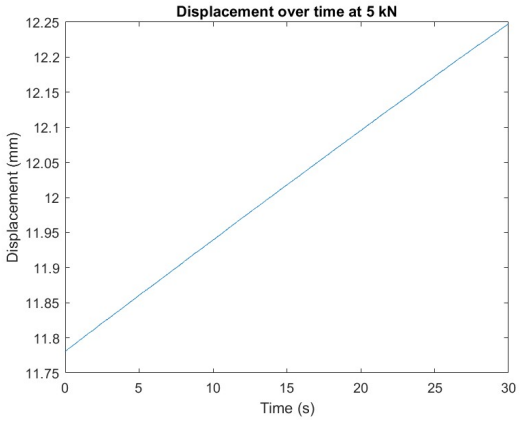

Figure 5.11: Displacement of the loading head of the Instron machine over time at 5 kN.

Finally, a possible explanation for the increase in results is related to both the variation in time of arrival of waves through water (figure 5.9) and possibly the variation in attenuation (figure 5.7). A possible explanation for the variation in time of arrival of waves through water is that the surface of the rope reflects more ultrasonic waves due to the increasing stiffness. A theoretical connection to the variation in attenuation is presented in Appendix B. However, this theory needs to be worked out and more research is required.

5.5.3. Discussion of stiffness and load assessment

The stiffness calculated according to the theory and presented in table 5.2 is presented as a complex stiffness. The complex stiffness consists of a storage modulus (real part) and a loss modulus (imaginary part) where the storage modulus is related to the instantaneous stiffness and the loss modulus is related to the viscoelastic effect. The storage modulus increases for higher applied values of load as well as the absolute value of the complex stiffness. This is according to the theory [47]. It should be noted that the literature value of DM20 is equal to 94GPa [9] which is slightly higher than the calculated values for the stiffness.

The calculated load shown in table 5.4 is higher for the actual applied load of 1kN while the calculated load is lower than the actual applied load for 2, 3, 4 and 5kN. This might be explained by the fact that the calculated stiffness is slightly lower than the literature value. Looking at formula 3.17, it is apparent that the stiffness has a smaller effect on the tension than the natural frequency due to the fact that the natural frequency is squared in this formula. Furthermore, it should be noted that the measured frequency increases much faster than the stiffness between two consecutive load levels. This means that an undervalued stiffness has a larger effect on 1kN actual applied load than on the higher actual applied load values.

Finally, it should be noted that formula 3.17 is derived based on the assumption that the test specimen is fully submerged in water which was not the case during the experiments. During the experiments, approximately 70% of the test specimen was submerged in water. When submerged in water, the test specimen experiences damping due to the added mass of the water. When only part of the test specimen is submerged, the boundary conditions for the formula change meaning that the derivation

of the formula is simplified. The effect is expected to be relatively small but it could partly explain the inaccuracy of the results with respect to the theoretical values.

5.6. Sensitivity analysis

There are different methods to perform a sensitivity analysis. In this case, two independent input values are measured (attenuation and frequency) during the experiments leading to two outputs (stiffness and load). Since the two input values are independent, it makes sense to use a One-at-a-time (OAT) approach. In this approach, one input variable is changed every time while keeping the other variables unchanged to see the effect on the output. The input variables are varied by $\pm 10\%$ in steps of 2%. This leads to the following variations in the input values for the factor $\frac{a}{a_0}$ (table 5.5) and frequency f_n (table 5.6).

Table 5.5: Median and variation of the $\frac{a}{a_0}$ factor for the sensitivity analysis.

	1kN	**2kN**	**3kN**	**4kN**	**5kN**
-10%	0.12	0.15	0.17	0.19	0.24
-8%	0.13	0.16	0.17	0.19	0.25
-6%	0.13	0.16	0.17	0.20	0.25
-4%	0.13	0.16	0.18	0.20	0.26
-2%	0.13	0.17	0.18	0.20	0.26
Median	0.14	0.17	0.19	0.21	0.27
+2%	0.14	0.17	0.19	0.21	0.27
+4%	0.14	0.18	0.19	0.21	0.28
+6%	0.14	0.18	0.20	0.22	0.29
+8%	0.15	0.18	0.20	0.22	0.29
+10%	0.15	0.19	0.20	0.23	0.30

Table 5.6: Median and variation of the frequency for the sensitivity analysis.

	1kN	**2kN**	**3kN**	**4kN**	**5kN**
-10%	115.00	135.00	155.00	180.00	195.00
-8%	117.56	138.00	158.44	184.00	199.34
-6%	120.11	141.00	161.89	188.00	203.67
-4%	122.67	144.00	165.33	192.00	208.00
-2%	125.22	147.00	168.78	196.00	212.34
Median	127.78	150.00	172.22	200.00	216.67
+2%	130.34	153.00	175.66	204.00	221.00
+4%	132.89	156.00	179.12	208.00	225.34
+6%	135.45	159.00	182.55	212.00	229.67
+8%	138.00	162.00	186.00	216.00	234.00
+10%	140.56	165.00	189.44	220.00	238.34

First, the effect of the variation of the $\frac{a}{a_0}$ factor on the stiffness is evaluated. The result may be found in table A.1 in Appendix A. Note that a variation of $\pm 10\%$ in the

$\frac{a}{a_0}$ factor yields only a 1% increase/decrease in the stiffness.
Next, it should be considered that the tension is dependent on the frequency (input) and the stiffness. The effect of variation of both the frequency and the stiffness is considered. First, the effect of the variation in stiffness on the tension is considered. This is done by using the stiffness from table A.1. The resulting tension is shown in table A.2. Note that the tension does not change significantly due to the variation in stiffness. The influence of the stiffness on the tension is negligible. It is however expected that the influence of the stiffness on the tension increases with increasing rope diameters. Secondly, the effect of variation in frequency on the tension is considered. The frequency is varied according to the values in table 5.6 per load level and the results can be found in table A.3. Note that a variation of $\pm 10\%$ in frequency yields an increase/decrease in tension of approximately $\pm 19\%$. Therefore it can be concluded that the calculated tension is very sensitive to changes in frequency input.

5.7. Chapter highlights

This chapter shows the results obtained from the experiments. The theoretical methodology described in chapter 3 was used to calculate the stiffness and the tension in the rope based on the attenuation coefficient and the natural frequencies measured by the ultrasonic transducers and the Laser Doppler Vibrometer respectively. It is concluded that the calculated stiffness is comparable to the literature value and shows the expected increasing trend for increasing load. Furthermore, it is concluded that the load can be recalculated based on the measurements and yields results that are increasingly more accurate for higher load values. At an applied load of 1 kN, the calculated load has an error of 30%, while at 5 kN, the calculated load has an error of 12%. It is concluded that the derivation of formula 3.17 assumes a fully submerged test specimen while in reality this was not the case during the experiments. This can explain the error between actual load and calculated load. Furthermore, it is noted that the calculated stiffness is slightly smaller than the literature value for the stiffness. This can contribute to the error between actual load and calculated load too.
Finally, it is noted that the results for the attenuation shown in figure 5.7 show an increasing spread in results for higher load values. Multiple possible reasons are presented. It is however expected that an increased scatter of the ultrasonic guided waves due to increasing stiffness in combination with a changing surface area faced by the ultrasonic transducers due to slip of the test specimen the most likely reason is.

6

Conclusions

A novel methodology for the in-situ, non-contact assessment of the structural health of synthetic fiber ropes is proposed in this research. In the conclusion, the main question will be answered. The main question is defined as follows.

"How can material properties and tension of synthetic mooring ropes be assessed using a non-contact combination of ultrasonic guided waves and vibration measurement?"

The main question shall be answered making use of four subquestions. The answers to the subquestions are listed below.

"What kind of test methodology can be used in order to measure wave propagation in a synthetic mooring line in a non-contact manner?"

The proposed test methodology uses the principle of attenuation of ultrasonic guided waves in HMPE ropes to find a complex wave number. The complex wave number is related to material properties such as the constant density and the variable stiffness. The methodology is based on propagation of ultrasonic guided waves. Underwater non-contact ultrasonic transducers are being used in order to measure the relevant properties of the ultrasonic guided wave such as attenuation coefficient. It was concluded that the proposed test methodology has the potential to accurately find the ultrasonic wave through water and through HMPE rope material. Furthermore, it was concluded that attenuation coefficients of an ultrasonic guided wave can be determined while being able to translate the attenuation coefficient to stiffness properties of the material.

"How can non-contact vibration measurements assess tension in synthetic mooring ropes?"

It was concluded that the Doppler principle can be used via the use of a Laser Doppler Vibrometer in order to assess tension in cables and thus in synthetic mooring ropes. The literature review showed that vibration measurement alone is insufficient in order to assess tension in mooring ropes since the tension is a function of frequency and stiffness. Therefore, it is important to determine the stiffness of the synthetic mooring

line too, especially since it was found that the stiffness of synthetic materials increase with increasing load. It was concluded that the combination of the two measuring techniques (ultrasonic guided waves and vibration measuring) is required.

”How does viscoelasticity affect ultrasonic wave propagation in synthetic mooring ropes?”

It is known that viscoelasticity has an effect on ultrasonic guided wave propagation. Especially the attenuation coefficient is dependent on the viscoelastic properties of the material as the attenuation coefficient is defined as a complex number due to the viscoelastic nature of the material where the real part is defined as the storage modulus and the imaginary part is defined as the loss modulus. For increasing loads, the stiffness of the material increases. Due to this increased stiffness, the attenuation coefficient lowers which affects the amplitudes of the received signals travelling through the rope specimen.

”How does tension affect ultrasonic wave propagation in synthetic mooring ropes?”

The tension in mooring ropes influences the stiffness of the mooring line. A higher tension leads to a higher stiffness. It was concluded that the higher stiffness causes a higher acoustic impedance. This higher acoustic impedance in its turn again causes a higher reflection coefficient of the material. This means that the ultrasonic waves are scattered away from the surface more when the load increases. When the ultrasonic waves scatter more from the surface, the spread in the results for the attenuation coefficient becomes larger. It was concluded that the larger spread in the attenuation coefficient did not have a significant influence on the calculated stiffness.

In conclusion, the material properties can, within margins, be assessed using non-contact ultrasonic guided waves. There are several factors for synthetic mooring ropes to which attention shall be paid when testing them using ultrasonic guided waves such as the fact that the material is viscoelastic and that the material stiffness changes with changing load. Combining the obtained stiffness values with non-contact vibration assessment leads to a methodology to estimate tension in synthetic mooring ropes.

7

Future Research

This chapter will provide recommendations for future research. This thesis showed the potential of the non-contact combination of assessment techniques to assess tension in mooring ropes, but more research is required.

7.1. Alternative methodology

The current methodology makes use of the attenuation coefficient in order to determine the stiffness of the material. However, it is also possible to take an alternative approach by measuring the wave speed of longitudinal, transverse and/or shear waves. This methodology has been shown to have high potential for other materials (such as steel and composite laminates) to determine stiffness properties. However, in this thesis, the measurements were not reliable enough to use this method due to the possibility of slightly shifting ultrasonic transducers during the experiment, changing their distance to the rope. The accuracy for these measurements needs to be very precise, meaning that small changes in distance between the rope and transducers between two different load levels can make the measurements unusable. It is recommended for future research to look at the potential of these kind of measurements over the attenuation-approach.

7.2. Improving test procedure

The test procedures need to be improved for future research. As mentioned, during the tests there has been the possibility of a shift in the transducers with respect to the rope. This can make measurements useless and therefore it is important to ensure that the transducers can not change position in the slightest way during the experiments. After the experiments, it was determined that wave speed of the wave part travelling through the specimen can not be determined accurately due to this possible shift of the transducers. To account for this, the literature value for the wave speed through the specimen has been used rather than actual calculated wave speeds. It is expected that the quality of the results is improved when the wave speed is determined via testing rather than using a reference value. It is therefore recommended to fix the suspension of the transducers to the tank to avoid unwanted movement in future research.

The knots in the synthetic mooring ropes have to be improved for future research as well. Knots tend to slip and in fact, any knot will always slip when subjected to enough tension. During the experiments, it was noticed that the slip would not decrease when subjected to load for a longer period of time. Similarly the slip would not decrease when subjected to a high load after then going back to a lower load level. This strengthens the believe that the slipping of the knot keeps forming an issue that can not be overcome in this configuration. Therefore, it is recommended to find an alternative way to tie the rope in a loop to the testing machine. A suggestion is to use a socket and fix the mooring rope in the socket using resin creating a loop. An alternative would be to use the so called splicing method which is common for similar tensile tests involving fiber ropes. With this method, part of the end of the rope is spliced to embed the end, forming a loop.

7.3. Future application

The current inspection method for synthetic offshore mooring ropes is visual inspection [15], but it was concluded that this is a time consuming, expensive and possibly dangerous method. On top of that, visual inspection is sometimes inadequate in finding damage [10]. In case this research is continued, it could be a good addition or alternative to the current inspection method. With this method, there is no need for divers to inspect the mooring ropes which would take away potential risks for divers and at the same time it has the potential to lower expenses for product owners in the long run. The proposed testing method could be used while the mooring ropes are fully in service. A proposed way to make use of this methodology would be by using an ROV. The underwater ultrasonic transducers could be fixed to an ROV while an LDV could be placed inside a watertight, transparent casing on the ROV. More research on this application of the methodology in service is however necessary.

Bibliography

[1] UNFCCC. The Paris Agreement - Publication. Paris Climate Change Conference - November 2015, November 2019.

[2] DNV. Energy transition outlook 2022, 2022. Retrieved from: https://www.dnv.com/energy-transition-outlook/download.html?utm_source=Google&utm_medium=Search&utm_campaign=eto22&gad=1&gclid=CjwKCAjw9J2iBhBPEiwAErwpeaArF5jBLM4yidlO_RgVurOrg-zbqP82ul-bPTUxozwmauogXDHI9RoCwLwQAvD_BwE.

[3] Windeurope. Offshore Wind in Europe. Key trends and statistics 2019, 2019. Retrieved from: https://windeurope.org/wp-content/uploads/files/about-wind/statistics/WindEurope-Annual-Offshore-Statistics-2019.pdf.

[4] C.V. Amaechi, A. Reda, H.O. Butler, I.A. Ja'e, and C. An. Review on Fixed and Floating Offshore Structures. Part I: Types of Platforms with Some Applications. *Journal of Marine Science and Engineering*, 10(8), 2022.

[5] DeepRope. Polyester & dyneema® mooring ropes manual 2004, 2004. Retrieved from: https://ocw.tudelft.nl/wp-content/uploads/deepropemanual.pdf.

[6] G.P. Foster. Advantages of fiber rope over wire rope. *Journal of Industrial Textiles*, 32(1):67–75, 2002.

[7] L. Johanning, H. Smith George, and J. Wolfram. Measurements of static and dynamic mooring line damping and their importance for floating wec devices. *Ocean Engineering*, 34(14):1918–1934, 2007.

[8] S.D. Weller, P. Davies, A.W. Vickers, and L. Johanning. Synthetic rope responses in the context of load history: Operational performance. *Ocean Engineering*, 83:111 – 124, 2014.

[9] S.D. Weller, L. Johanning, P. Davies, and S.J. Banfield. Synthetic mooring ropes for marine renewable energy applications. *Renewable Energy*, 83:1268–1278, 2015.

[10] K. Ma, H. Shu, P. Smedley, D. Lapos-Hostis, and A. Duggal. A historical review on integrity issues of permanent mooring systems. 2013.

[11] A. Kvitrud. Lessons learned from norwegian anchor line failures 2010-2013. *Proceedings of OMAE 2014 33th International Conference on Ocean, Offshore and Arctic Engineering*, June 2014.

[12] K. Arne. Anchor line failures- norwegian continental shelf - 2010-2014, 2014.

[13] B. Patel. Engineering Fit-For-Purpose Dyneema® Ropes for the Stiesdal TetraSpar Demonstrator, March 2022.

[14] R. Bosman, Q. Zhang, A. Leao, and C. Godreau. First Class Certification on HMPE Fiber Ropes for Permanent Floating Wind Turbine Mooring System. In *OTC-30475-MS*, 2020.

[15] DNV. DNV-RP-E304: Damage assessment of fibre ropes for offshore mooring, 2019. Retrieved from: https://www.dnv.com/oilgas/download/dnv-rp-e304-damage-assessment-of-fibre-ropes-for-offshore-mooring.html.

[16] R. Balaji, S.A. Sannasiraj, and V. Sundar. A load cell for the measurement of slack mooring forces. *Journal of The Institution of Engineers (India): Series C*, 2014.

[17] R. Yan, X. Chen, and S. Mukhopadhyay. *Structural health monitoring*. Springer, 2017.

[18] Corewind. D2.1 Review of the state of the art of mooring and anchoring designs, technical challenges and identification of relevant DLCs, 2020. retrieved from: https://corewind.eu/wp-content/uploads/files/publications/COREWIND-D2.1-Review-of-the-state-of-the-art-of-mooring-and-anchoring-designs.pdf.

[19] S. Ford, A. La Grotta, H. Rasul, R. Arnau, M. Campo-Cossío, A. Puras, J. Sainz, J. Rodríguez, J. Fernandez, T. Hunter, J. Basurko, I. Elorza, and N. Fonseca. Mooring system integrity management through monitoring, digital twin and control technologies for cost reduction and increased efficiency. 2020.

[20] Omega. What are load cells and how do they work?, 2019. https://www.omega.com/en-us/resources/load-cells. Last accessed 28 July 2023.

[21] G. Drummond, J.F. Watson, and P.P. Acarnley. Acoustic emission from wire ropes during proof load and fatigue testing. *NDT & E International*, 40(1):94–101, 2007.

[22] P. Nagy. Longitudinal guided wave propagation in a transversely isotropic rod immersed in fluid. *The Journal of the Acoustical Society of America*, 98(1):454–457, 07 1995.

[23] A. Mehrabi and S. Farhangdoust. A laser-based noncontact vibration technique for health monitoring of structural cables: Background, success, and new developments. *Advances in Acoustics and Vibration*, 2018:1–13, June 2018.

[24] C. Sheng, G. He, Z. Hu, C. Chou, J. Shi, J. Li, Q. Meng, X. Ning, L. Wang, and F. Ning. Yarn on yarn abrasion failure mechanism of ultrahigh molecular weight polyethylene fiber. *Journal of Engineered Fibers and Fabrics*, 16, 2021.

[25] M. Vlasblom, J. Boesten, S. Leite, and P. Davies. Development of HMPE Fiber for Permanent Deepwater Offshore Mooring. All Days, April 2012.

[26] S. Sørum, N. Fonseca, M. Kent, and R. Faria. Assessment of nylon versus polyester ropes for mooring of floating wind turbines. *Ocean Engineering*, 278, 2023.

[27] Y. Chevillotte, Y. Marco, G. Bles, K. Devos, M. Keryer, M. Arhant, and P. Davies. Fatigue of improved polyamide mooring ropes for floating wind turbines. *Ocean Engineering*, 199, 2020.

[28] M. Wehr, A. Pott, and K. Wehking. *Bending Fatigue Strength and Lifetime of Fiber Ropes*, pages 73–84. July 2018.

[29] P. Davies, N. Lacotte, M. Arhant, D. Durville, A. Belkhabbaz, M. François, F. Khouri, K. Konate, S. Mills, J. Philippe, C. DeFrance, P. Smeets, D. Sherman, K. Newboles, A. Ledoux, N. Chazot, S. Saillard, R. Kante, D. Cannell, and O. Lodeho. Improved Bend Over Sheave Durability of HMPE Ropes for Deep Sea Handling. June 2018.

[30] A.R Bunsell, J.M. Herrera Ramirez, and C. Le Clerc. Tensile fatigue of thermoplastic fibers. In *Handbook of Properties of Textile and Technical Fibres (Second Edition)*, pages 595–618. Woodhead Publishing, second edition edition, 2018.

[31] M. C. Kenney, J. F. Mandell, and F. J. McGarry. Fatigue behaviour of synthetic fibres, yarns, and ropes. *Journal of Materials Science*, 1985.

[32] J.F. Mandell. Modeling of marine rope fatigue behavior. *Textile Research Journal.*, 1987.

[33] Y. Chevillotte, Y. Marco, G. Bles, K. Devos, M. Keryer, M. Arhant, and P. Davies. Fatigue of improved polyamide mooring ropes for floating wind turbines. *Ocean Engineering*, 199, 2020.

[34] M. Seo, H. C. Wu, J. Chen, C. S. Toomey, and S. Backer. Wear and fatigue of nylon and polyester mooring lines. *Textile Research Journal*, 67(7):467–480, 1997.

[35] C. Humeau, P. Davies, P. Smeets, T.A.P. Engels, L.E. Govaert, M. Vlasblom, and F. Jacquemin. Tension fatigue failure prediction for HMPE fibre ropes. *Polymer Testing*, 65:497–504, 2018.

[36] P. Smeets, M. Jacobs, and M. Mertens. Creep as a design tool for hmpe ropes in long term marine and offshore applications. In *MTS/IEEE Oceans 2001. An Ocean Odyssey.*, volume 2, pages 685–690 vol.2, 2001.

[37] M. Vlasblom, J. Boesten, S. Leite, and P. Davies. Creep and stiffness of hmpe fiber for permanent deepwater offshore mooring. In *2012 Oceans - Yeosu*, pages 1–7, 2012.

[38] S. Weller, P. Davies, L. Johanning, and S. Banfield. *Guidance on the use of synthetic fibre ropes for marine energy devices Deliverable 3.5.2 from the MERiFIC Project*. 2013.

[39] M. Vlasblom. The manufacture, properties, and applications of high-strength, high-modulus polyethylene fibers. In *Handbook of Properties of Textile and Technical Fibres (Second Edition)*, The Textile Institute Book Series, pages 699–755. Woodhead Publishing, second edition edition, 2018.

[40] C.C. Huang, H.J. Tang, and B.S. Wang. Numerical modeling for an in situ single-point-mooring cage system. *Oceanic Engineering, IEEE Journal of*, 35:565 – 573, August 2010.

[41] J. Baker, S. Yim, E. Amon, S. Moran, T. Lettenmaier, and A. von Jouanne. Numerical and experimental analysis of the ocean sentinel mooring system to enable improved modeling and design. *Proceedings of the 2nd Marine Energy Technology Symposium*, April 2014.

[42] N.F. Casey, K.M. Holford, and J.L. Taylor. The acoustic evaluation of wire ropes immersed in water. *NDT International*, 20(3):173–176, 1987.

[43] N.F. Casey, H. White, and J.L. Taylor. Frequency analysis of the signals generated by the failure of constituent wires of wire rope. *NDT International*, 18(6):339–344, 1985.

[44] M. Berliner and R. Solecki. Wave propagation in fluid-loaded, transversely isotropic cylinders. Part I. Analytical formulation. *The Journal of the Acoustical Society of America*, 99(4):1841–1847, April 1996.

[45] M. Berliner and R. Solecki. Wave propagation in fluid-loaded, transversely isotropic cylinders. Part II. Numerical results. *The Journal of the Acoustical Society of America*, 99(4):1848–1853, 04 1996.

[46] V. Dayal. Longitudinal waves in homogeneous anisotropic cylindrical bars immersed in fluid. *The Journal of the Acoustical Society of America*, 93(3):1249–1255, March 1993.

[47] P. Davies, M. Franois, F. Grosjean, P. Baron, K. Salomon, and D. Trassoudaine. Synthetic mooring lines for depths to 3000 meters. *Proceedings of the Annual Offshore Technology Conference*, May 2002.

[48] R. Raišutis, R. Kažys, L. Mažeika, E. Žukauskas, V. Samaitis, and A. Jankauskas. Ultrasonic guided wave-based testing technique for inspection of multi-wire rope structures. *NDT & E International*, 62:40–49, 2014.

[49] S. Waluyo. *A modelling approach to ultrasound evaluation of material properties*. PhD thesis, University of Missouri, 2010.

[50] S.A. Silling. Attenuation of waves in a viscoelastic peridynamic medium. *Office of Scientific and Technical Information*, 2019.

[51] I. S. Grigoriev and E. Z. Meĭlikhov. *Handbook of physical quantities*. CRC Press, Moscow, 1997.

[52] C.H. Kim, B.W. Jo, and J.T. Jun. Application of laser vibrometer to the measurement and control of cable tensile forces in cable-stayed bridges. *International Journal of Distributed Sensor Networks.*, 2012.

[53] Q. Han, Y. Ma, W. Xu, Y. Lu, and A. Cheng. Dynamic characteristics of an inclined flexible cylinder undergoing vortex-induced vibrations. *Journal of Sound and Vibration*, 394:306–320, 2017.

[54] DNV. Recommended Practive DNV-RP-C205, Environmental conditions and environmental loads. *Det Norske Veritas*, 2019.

[55] X. Li. Fundamental of fibers. In *Cut Protective Textiles*, The Textile Institute Book Series, pages 59–110. Woodhead Publishing, 2020.

[56] RS PRO SDG1032X Waveform Generator, 30MHz Max - RS Calibrated. https://nl.rs-online.com/web/p/arbitrary-waveform-generators/1882691.

[57] WMA-300 High speed high voltage amplifier. https://www.falco-systems.com/High_voltage_amplifier_WMA-300.html.

[58] VS150-WIC-V01. https://www.vallen.de/sensors/watertight-sensors/vs150-wic-v01-2/.

[59] AMSY-6 System Specification. https://www.vallen.de/zdownload/pdf/AMSY-6_Spec.pdf.

[60] OFV-505 Sensor Head Datasheet. https://www.atecorp.com/atecorp/media/pdfs/data-sheets/polytec-ofv-505.pdf?ext=.pdf.

[61] User Manual - Laser Vibrometer - OFV. https://pearl-hifi.com/06_Lit_Archive/05_LDV/Polytec_Hardware_Manuals/OFV_303/OFV_2200_303_353.pdf.

[62] Micsig - Tablet Oscilloscope - Quick Guide. https://www.batronix.com/files/Micsig/tBook/tBook-quick-guide-and-safety-information.pdf.

[63] Instrumented Impact Hammer IH-02 - 2kN Range. https://www.djbinstruments.com/products/instrumentation/impact-hammers/view/ih-02.

[64] L. Pahlavan. *Wave Propagation in Thin-walled Composite Structures: Application to Structural Health Monitoring*. PhD thesis, Delft University of Technology, 2012.

[65] CSL. A compilation on high modulus polyethylene fibers. 2010.

[66] A. Franck. Viscoelasticity and dynamic mechanical testing. *TA Instruments Germany*, 2001.

[67] A. Kumar, P.P. Pathak, and N. Dass. A study of speed of sound in water. *IOSR Journal of Applied Physics*, 08:21–23, 2016.

[68] K. Raum. Microelastic imaging of bone. *IEEE transactions on ultrasonics, ferroelectrics, and frequency control*, 55:1417–31, 2008.

A

Sensitivity Analysis

This appendix shows part of the tables with the data used for the sensitivity analysis in section 5.6.

Table A.1: Variation in stiffness for a variation of the $\frac{a}{a_0}$ factor between $\pm 10\%$ from the median.

	1kN	2kN	3kN	4kN	5kN
-10%	84.53 +39.65i	87.00 +36.21i	87.97 +34.72i	89.18 +32.74i	91.60 +28.17i
-8%	84.79 +39.30i	87.24 +35.86i	88.20 +34.36i	89.40 +32.37i	91.79 +27.77i
-6%	85.04 +38.98i	87.47 +35.50i	88.43 +34.00i	89.61 +31.99i	91.97 +27.38i
-4%	85.28 +38.65i	87.70 +35.16i	88.64 +33.64i	89.81 +31.63i	92.15 +27.00i
-2%	85.52 +38.33i	87.92 +34.81i	88.85 +33.29i	90.01 +31.27i	92.32 +26.62i
Median	85.75 +38.01i	88.13 +34.48i	89.06 +32.95i	90.20 +30.92i	92.49 +26.24i
+2%	85.98 +37.69i	88.34 +34.14i	89.26 +32.61i	90.34 +30.57i	92.65 +25.88i
+4%	86.20 +37.39i	88.54 +33.82i	89.45 +32.27i	90.57 +30.22i	92.80 +25.52i
+6%	86.41 +37.08i	88.73 +33.49i	89.64 +31.94i	90.75 +29.89i	92.95 +25.16i
+8%	86.62 +36.78i	88.92 +33.18i	89.82 +31.62i	90.92 +29.55i	93.10 +24.81i
+10%	86.82 +36.48i	89.11 +32.86i	89.99 +31.30i	91.08 +29.22i	93.24 +24.47i

Table A.2: Variation in tension for the variation of the stiffness from table A.1.

1kN	2kN	3kN	4kN	5kN
1301.7	1847.5	2517.6	3522.2	4422.7
1301.7	1847.5	2517.6	3522.2	4422.7
1301.7	1847.5	2517.6	3522.2	4422.7
1301.7	1847.5	2517.6	3522.2	4422.7
1301.7	1847.5	2517.6	3522.2	4422.7
1301.7	1847.5	2517.6	3522.2	4422.7
1301.7	1847.5	2517.6	3522.2	4422.7
1301.7	1847.5	2517.6	3522.2	4422.7
1301.7	1847.5	2517.6	3522.2	4422.7
1301.7	1847.5	2517.6	3522.2	4422.7
1301.7	1847.5	2517.6	3522.2	4422.7

Table A.3: Variation in tension for the variation of the frequency by $\pm 10\%$.

	1kN	2kN	3kN	4kN	5kN
-10%	1054.4	1496.5	2039.3	2853.0	3582.4
-8%	1101.8	1563.7	2130.9	2981.2	3743.4
-6%	1150.2	1632.5	2224.6	3112.2	3907.9
-4%	1199.7	1702.7	2320.2	3246.1	4075.9
-2%	1250.2	1774.3	2417.9	3382.8	4247.5
Median	1301.7	1847.5	2517.6	3522.2	4422.7
+2%	1354.3	1922.1	2619.3	3664.5	4601.4
+4%	1407.9	1998.3	2723.0	3809.6	4783.6
+6%	1462.6	2075.9	2828.8	3957.6	4969.3
+8%	1518.3	2154.9	2936.5	4108.3	5158.6
+10%	1575.1	2235.5	3046.3	4261.9	5351.4

B

Theory on spread in attenuation results

A potential theory on the spread in the results for the ultrasonic guided waves for higher load values is that the increasing stiffness of the test specimen yields an increased scatter of the ultrasonic waves. Raum (2008) [68] showed that materials with higher stiffness have a higher acoustic impedance which is shown in figure B.1.

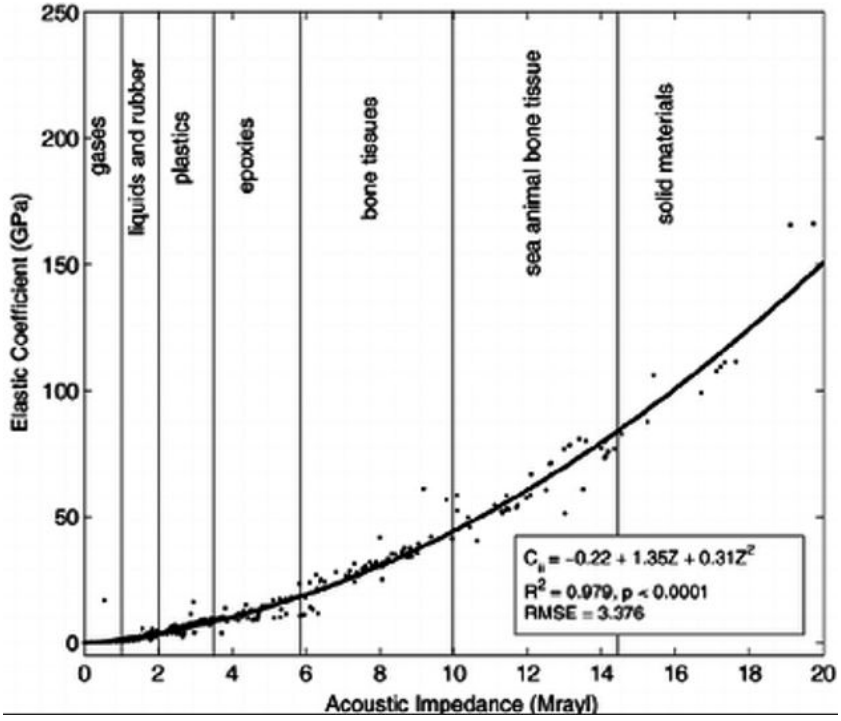

Figure B.1: Relation between acoustic impedance and stiffness [68].

This result is important as Raum also showed that a higher acoustic impedance yields a higher reflection coefficient. Increasing stiffness therefore means that ultrasonic waves are reflected of the surface more. It was shown in figure 2.4 that higher loads yield higher stiffness for HMPE ropes. This leads to the conclusion that ultrasonic waves are reflected more from the surface of the rope when the load increases which could possibly explain the fact that the variation in the results increases for

higher load levels. This is first of all apparent from figure 5.9 where the time of arrival of the wave travelling through water is shown. This figure shows the same variation in results and the fact that there is increased scatter due to a change in stiffness can explain this variation. This is due to the fact that the transmitter is close to the rope and a large part of the transmitted wave is therefore interacting with the rope. When a wave is reflected from the surface, the wave will propagate in a random direction which is unpredictable due to the irregularity of the outer surface of the rope. When the waves are scattered of the surface, the path they travel towards the receiver changes which results in slight differences in the distance travelled for each individual wave. This leads to a variation in time of arrival of the wave travelling through water. Looking at figure 5.5 and 5.6, it can be seen that the same variation in results is apparent. These are however resulting amplitudes of the part of the wave travelling through the rope rather than the time of arrival. The explanation for this might lie in the increasing acoustic impedance of the material as well. An increasing acoustic impedance does not only mean that there is increased scatter, it also means that there is less transmittance of the wave from one medium into the other. When looking at the path the sound waves travel from the transmitter, through the rope to either one of the receivers, there are two interfaces. First, the wave travels through water and meets the interface of the rope. Next, when leaking from the rope to the receivers, there is another interface the wave has to overcome namely the rope-water interface. With an increased impedance, the waves travelling inside the rope are transmitted to the water (and thus the receivers) more difficult. Transmittance and reflection is however a random process which also depends on the outer, irregular surface of the rope. Therefore, the amplitude of the transmitted wave could differ slightly between individual measurements. This could explain why there is a larger spread in results for higher load values. More research is required to validate this theory.